ABSTRACT

HUGHES, STEPHANIE CRISTINA. Electrochemical Studies of Neuroactive Molecules with Fast-Scan Cyclic Voltammetry at Carbon-Fiber Microelectrodes. (Under the direction of Dr. Leslie A. Sombers.)

Understanding the chemical dynamics of neuroactive molecules is critical to understanding the mechanisms underlying neurodegenerative disease states such as Parkinson's Disease (PD). Electrochemical techniques are well-suited to monitor the chemical dynamics of neuroactive molecules. In particular, fast-scan cyclic voltammetry (FSCV) at carbon-fiber microelectrodes is a prominent neuroanalytical tool that combines unparalleled micron spatial resolution and sub-second temporal resolution to monitor dynamic changes in neuroactive molecules in real-time to elucidate the chemical dynamics that underlie brain function and dysfunction in neurodegenerative disease states such as PD. This research aims to provide the framework for developing and modifying analytical tools to monitor neuroactive molecules such as nitric oxide (NO), and builds upon current techniques to monitor dopamine (DA) dynamics following pharmacological treatment with L-3,4-dihydroxyphenylalanine (L-DOPA) in living brain tissue in real-time.

NO is a highly reactive free radical reactive nitrogen species (RNS) that has been implicated in the pathogenesis and progression of PD. NO quickly reacts to produce more aggressive RNS such at peroxynitrite that interrupt normal cell signaling and ultimately lead to cell death. In this study, FSCV at carbon-fiber microelectrodes was used to detect NO *in vitro* with a well-established waveform. The use of Nafion-coated carbon-fiber microelectrodes enhanced the detection of NO. Future studies examining NO with FSCV should focus on optimizing FSCV parameters to better-resolve the voltammetric signature of NO in addition to establishing selectivity against common interferents both *in vitro* and in

brain slice tissue. In the future, this approach will enable the detection of NO in living tissue capable of addressing the role of RNS such as NO, in oxidative stress in PD.

The effects of L-DOPA on DA dynamics from single pulse electrical stimulations, as well as artificial phasic stimulation paradigms in striatal brain slices were assessed. In the presence of 50 μM L-DOPA the ability to detect DA at Nafion-coated carbon-fiber microelectrodes *in vitro* was hindered and caused irreversible fouling of the electrode. A more clinically relevant dose of L-DOPA (1 μM) significantly increased electrically-evoked DA release at Nafion-coated carbon-fiber microelectrodes in a phasic firing paradigm. Release and reuptake parameters of DA by way of the DA transporter (DAT) were assessed and DA reuptake was decreased following a more clinically relevant dose of L-DOPA. This work builds on the understanding DA release and reuptake dynamics following L-DOPA treatment and will provide the foundation to assess the effects of L-DOPA on DA release and reuptake parameters in Parkinsonian animals to build a more complete picture of the chemical dynamics underlying neurodegenerative disease states such as PD.

Electrochemical Studies of Neuroactive Molecules with Fast-Scan Cyclic Voltammetry at Carbon-Fiber Microelectrodes

by
Stephanie Cristina Hughes

A thesis submitted to the Graduate Faculty of
North Carolina State University
in partial fulfillment of the
requirements for the degree of
Master of Science

Chemistry

Raleigh, North Carolina

2013

APPROVED BY:

_____	_____
Dr. Leslie A. Sombers Committee Chair	Dr. Gregory S. McCarty
_____	_____
Dr. Morteza G. Khaledi	Dr. Kenneth W. Hanck

BIOGRAPHY

And whatever you do, do it heartily, as to the Lord and not to men.

-Colossians 3:23

ACKNOWLEDGMENTS

There are many individuals that I wish to thank for the help and support they have given me during my time at NC State. First, I would like to thank the wonderful professors I have had in my graduate classes. It was a privilege to learn from each and every one of them. I would also like to acknowledge my undergraduate mentors, Dr. Carol M. Babyak and Dr. B.J. Yoblinski for continuing to encourage me and mentor me throughout my undergraduate and graduate careers. I would like thank the members of my examining committee, Dr. Leslie Sombers, Dr. Gregory McCarty, Dr. Morteza Khaledi, and Dr. Kenneth Hanck for taking the time to read this thesis.

Thank you to the entire Sombers lab, I cannot imagine a better group of people to work with. I especially would like to thank Dr. Marina Spanos who reviewed this document with unbelievable attention to detail. I appreciate your hard work and relentless encouragement and I am so grateful to have made such a wonderful friend and mentor. Thank you for helping me the whole way through and for helping me to realize my dreams! I would also like to thank Leyda Lugo Morales who also helped review this document and provided me with insight throughout each one of my projects and who also taught me many invaluable lessons in science. I am thankful for your friendship! I do not know how I would have gotten any brain slice experiments to work without Dr. James Roberts, who not only taught me but helped me prepare for each and every brain slice experiment. Not only that, thank you for your insight each time I met a brick wall. Thank you to Julie Gras-Najjar who also helped review this document and is a phenomenal friend. Thank you for the talks and

coffee walks. Thank you to Hadeer Metwally and Rochana Jayakumar for sticking it out with me through each one of my projects, you guys are the best!

I would like to thank my parents, Steve and Emma Hughes and my sisters, Stacey and Susan for all of their support throughout each and every moment of my life. I am so very thankful that I have the most wonderful family, a gift that could have only come from God. I would also like to thank Samantha Blake, Deanna Tesch, Phil Loziuk, Erik Loomis, Diane McClary, Ashley Accursio, David Bowman, Nick Merrill, Christer Akouala and Bethany Carter whose friendships mean so very much to me. Thank you to my Cataloochee Ski Patrol Family for always having my back and keeping me sane. Thank you especially to Chase White for believing in me and for supporting me through thick and thin, even when I didn't think I could continue. You constantly remind me that there is a greater purpose to everything.

I would like to give a very special thanks to Dr. Erin Banks who believed in me each and every day. Thank you for the impact you have had on my career. I am so thankful for you and the IMSD program at NC State. You all are like family and this is all because of Dr. Banks. Thank you so much for all of the meetings and talks and checking in on me and thank you for always building me up. You have taught me so much.

The person who I am most indebted to is my advisor Dr. Leslie A. Sombers. I don't think I could have survived this journey without your help, support and patience. Thank you for helping to mold me into the scientist I am today. I am honored to have had the opportunity to work in your laboratory alongside so many amazing scientists.

TABLE OF CONTENTS

LIST OF EQUATIONS

CHAPTER 2 EQUATIONS:

CHAPTER 3 EQUATIONS:

LIST OF FIGURES

CHAPTER 1:

CHAPTER 2:

CHAPTER 3:

CHAPTER 1

Electrochemical Measurements of Biological Molecules

1.1 Chemical Communication in the Brain

Neurons are the fundamental components of the nervous system. Communication between neurons occurs via the synapse by means of chemical messengers known as neurotransmitters. Action potentials begin at the neuron's axon hillock and are generated from the opening and closing of sodium (Na^+) and potassium (K^+) ion-gated channels. At a resting membrane potential, these ion-gated channels are closed. Depolarization of the resting membrane potential causes ion-gated channels to open allowing the influx of Na^+. The membrane potential then continues to rise and current increases until all available Na^+ ion-gated channels are opened. Following a change in polarity of the membrane, Na^+ ion-gated channels are closed and Na^+ ions are actively transported out of the cell, activating K^+ ion-gated channels. This generates an efflux of K^+ and restores the resting membrane potential. This depolarization causes neurotransmitters to be released from synaptic vesicles via exocytosis. Once expelled into the synaptic cleft, neurotransmitters diffuse away from the presynaptic neuron and bind to receptors on the post synaptic neuron to other neurons to propagate the message.[1]

1.2 Dopamine Synthesis

Dopamine (DA) is a monoamine neurotransmitter that is involved in the regulation of motor behavior, reward and motivation through interacting brain nuclei such as the mesolimbic, nigrostriatal and tuberinfundibular dopaminergic pathways.[2] The amino acid tyrosine is the first precursor molecule in the biological synthesis of DA. Tyrosine is

hydroxylated to L-dihydroxyphenylalanine (L-DOPA) by the enzyme tyrosine hydroxylase (TH). L-DOPA is then decarboxylated to form DA by aromatic L-amino acid decarboxylase (AADC), interchangeably called DOPA decarboxylase. The rate-limiting step for the formation of DA is the enzymatic activity of TH, thus DA formation will only proceed at the rate of the conversion of tyrosine to L-DOPA.[1] A schematic of the synthesis of DA from tyrosine is shown in Figure 1.1.

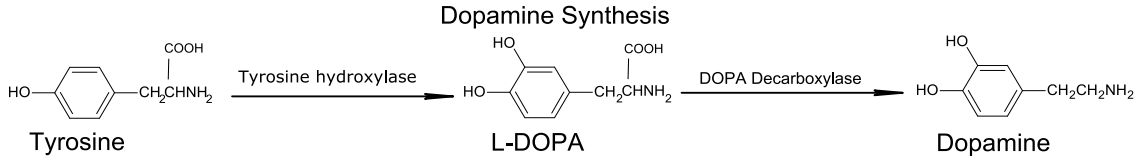

Figure 1.1 Synthesis of Dopamine. Tyrosine is converted to L-DOPA via the enzyme tyrosine hydroxylase. L-DOPA is then converted to DA via DOPA decarboxylase. Synthesis is limited by the activity of tyrosine hydroxylase.

Once synthesized, DA must be packaged into synaptic vesicles. This is accomplished by way of a protein called vesicular monoamine transporter (VMAT). When a cell is activated, depolarization triggers an influx of calcium ions into the synaptic terminal. This causes vesicles containing DA to fuse to the cell membrane and expel their contents into the extracellular space via exocytosis.[1]

1.3 Dopamine Reuptake and Catabolism

DA reuptake and catabolism are controlled by several mechanisms. The majority of DA released into the synaptic cleft is recycled. It is actively transported back across the neuronal membrane into the presynaptic terminal, via the DA transporter (DAT). Alternatively, DA can be catabolized through enzymatic reactions.[3] The primary enzymes responsible for the metabolism of DA are catechol-o-methyl transferase (COMT) and monoamine oxidase (MAO). COMT is present in the brain in non-neuronal compartments, whilst MAO is found intracellularly; the pathway of DA catabolism will depend on the location where breakdown takes place.[3,4] COMT and/or MAO break DA down into various metabolites including 3-methoxy-4-hydroxyphenethylamine (3-MT), 3,4-dihydroxyphenylacetic acid (DOPAC) and 3-methoxy-4-hydroxyphenylactic acid (HVA) also called homovanillic acid. A schematic of the pathways for DA catabolism is shown in Figure 1.2. In addition to reuptake and catabolism mechanisms, DA release is regulated by receptors and autoreceptors expressed on post and pre-synaptic neurons, respectively. These act to regulate neuronal function through feedback loops.

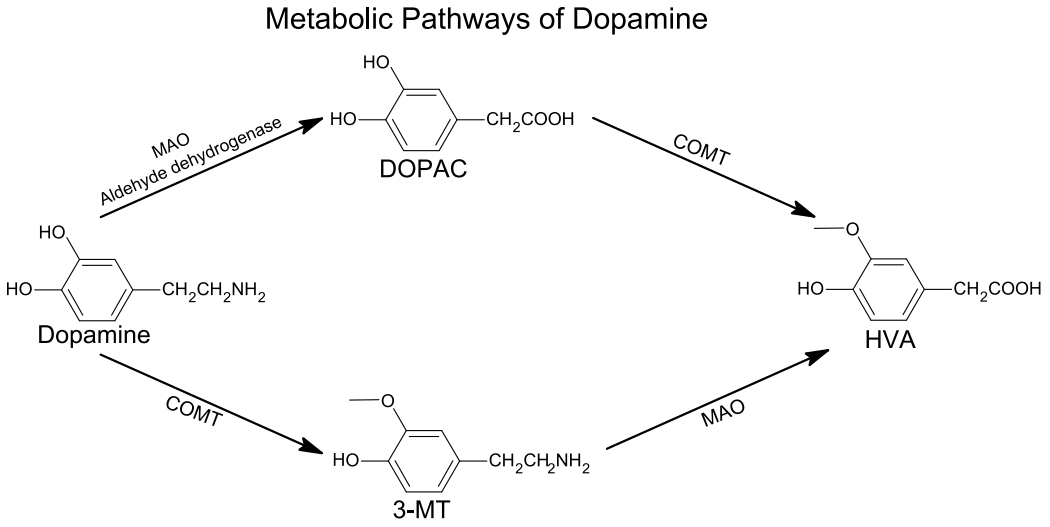

Figure 1.2 Metabolic Pathways of Dopamine. DA is converted to DOPAC via monoamine oxidase (MAO) and aldehyde dehydrogenase. Catechol-o-methyl transferase (COMT) will then metabolize DOPAC to homovanillic acid (HVA). Similarly, COMT will metabolize DA to 3-methoxy-4-hydroxyphenethylamine (3-MT). MAO will then metabolize 3-MT into HVA

1.4 Neurodegeneration

The progressive loss of neurons or nerve function is known as neurodegeneration and is seen in such diseases as Parkinson's disease (PD) and Alzheimer's disease (AD). Cell death proceeds by means of two dominate mechanisms, apoptosis, necrosis, or a combination of both. Programmed cell death or apoptosis, is genetically directed and used to remove cells that no longer function or are damaged beyond repair. Although cells may enter apoptosis naturally, cells can be forced into apoptosis when toxins, DNA damage, and oxidative stress cause the cell to improperly function triggering a cascade of chemical messages inducing cell death.[5] Necrosis is cell death that arises in response to external factors. Neurons that are destroyed through these processes are not regenerated. This often results in terminal

neurodegenerative disease states characterized by various symptoms according to the area of the brain affected or physical symptoms that present.[6]

1.5 Parkinson's Disease

Neurodegenerative diseases affect more than a million Americans. PD is the second most common neurodegenerative disorder, and typically affects people beginning in their sixties.[7,8] The Parkinson's Disease Foundation has determined that approximately 60,000 individuals are diagnosed with PD in the United States annually. The clinical manifestations associated with PD include rigidity, resting tremor, bradykinesia (slow movement), akinesia (lack of movement) and dyskinesia (involuntary movements).[9] The disease was first described in 1817 by James Parkinson in a discourse entitled "An Essay on the Shaking Palsy", though PD was not formally named until some 60 years later by Jean-Martin Charcot.[10,11] PD is characterized by a selective loss of dopaminergic cell bodies in the substantia nigra (SN) that project to the dorsal striatum.[12,13] This neural circuit is known as the nigrostriatal dopaminergic pathway and is critical to motor movement.[14] The neuronal circuitry involved in PD is depicted in a rodent model in Figure 1.3.

Once symptoms present in PD patients, as much as 85 % of dopaminergic projections from the SN to the dorsal striatum are irreversibly destroyed.[15] The remaining DA neurons can compensate for this loss to a certain extent by increasing their firing rate.[16] However, once a certain level of DA denervation has occurred, the remaining neurons cannot maintain dopaminergic tone and thus the characteristic PD motor symptoms begin to present.

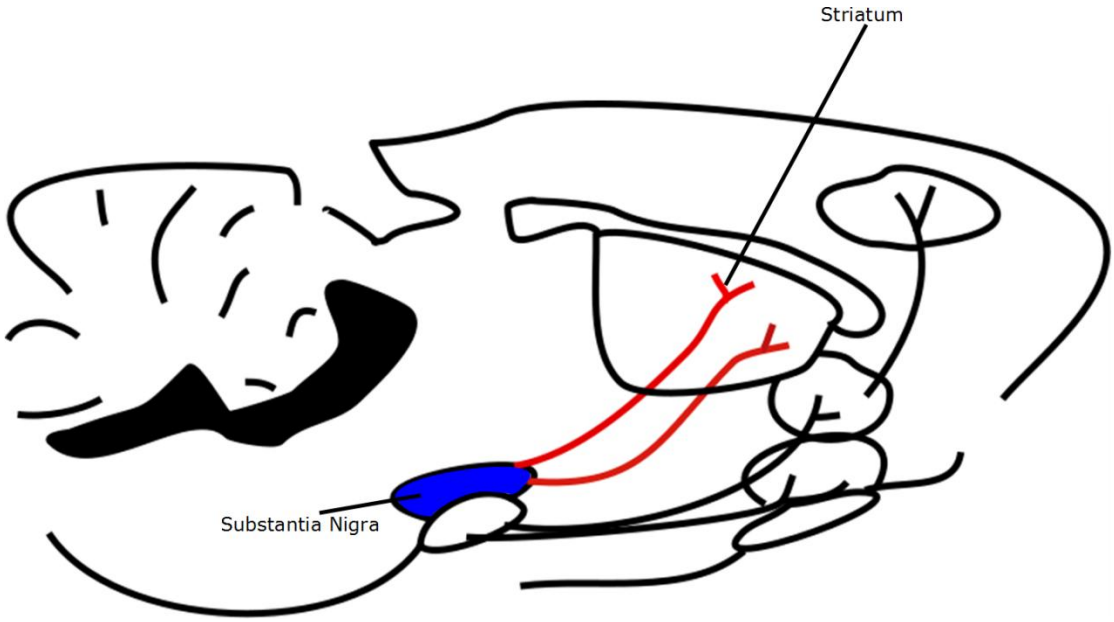

Figure 1.3 Nigrostriatal Dopaminergic Pathway in the rat brain is depicted above as a cartoon representation with the cerebellum to the left and the cerebrum to the right. The nigrostriatal pathway projects from the substantia nigra (SN), shown in blue, to the dorsal striatum, the upper neuronal circuit depicted above.

1.6 Oxidative Stress and Parkinson's Disease

The cause of PD remains elusive; however there are various hypotheses linking oxidative stress to the pathogenesis and progression of the disease.[7, 17] The oxidative stress hypothesis proposes that oxidative molecules present in the brain are responsible for causing an increase in oxidant species that induce subsequent damage. These reactive oxygen species (ROS) and reactive nitrogen species (RNS) include superoxide, nitric oxide, peroxynitrite and hydrogen peroxide (H_2O_2). They are capable of oxidizing molecules, including DA, to form quinones and other species that are broken down into radicals, leading to cellular dysfunction and ultimately cell death.[17, 18] Furthermore, analysis of post-mortem tissue

samples show increased iron concentrations in the SN of patients with PD, suggesting that Fenton chemistry contributes to oxidative stress and the formation of damaging radicals in this brain region.[7]

It is difficult to detect radical species due to short half-lives and rapid diffusion times, thus direct evidence for the role of oxidative stress in PD is lacking. Some indirect evidence comes from common animal models of PD, which are widely used research tools. Neurotoxins such as 6-hydroxydopamine (6-OHDA), 1-methyl-4-phenyl-1, 2, 3, 6-tetrahydropyridine (MPTP), rotenone and paraquat can be used to selectively destroy DA neurons and cause a Parkinsonian-like state.[19] It is hypothesized that the oxidation of the toxins generates ROS and paraquinones that cause DA denervation.[18,20] Radical species such as Nitric oxide (NO) can react with ROS (such as superoxide radical) to form peroxynitrite, a powerful oxidizing agent that breaks down into other radical species.[20] Furthermore, the expression of the enzyme responsible for the synthesis of NO, nitric oxide synthase (NOS), is increased in the SN in PD.[21] The excessive production of ROS and RNS that lead to oxidative stress can also oxidize integral proteins, lipids and DNA within neurons leading to their death.[7]

Mitochondrial dysfunction has also been hypothesized to play a role in the pathogenesis of PD. The origin for this hypothesis stems from studies using the neurotoxin MPTP, one of the classic PD model toxins known as a mitochondrial poison.[20] The mechanism that leads to mitochondrial dysfunction occurs when MPTP crosses the blood-brain-barrier and is converted to 1-methyl-4-phenylpyridinium (MPP^+) in the SN by the enzyme MAO. It is actively transported into DA cells by the DAT and subsequently

concentrated in mitochondria, where it can inhibit Complex I.[22] The inhibition of mitochondrial Complex I can deplete the levels of adenosine triphosphate (ATP). This leads to oxidative stress by way of the increased production of ROS, such as superoxide, which can be converted to H_2O_2.[22, 23] A schematic demonstrating the production of ROS and oxidative stress in mitochondria is shown in Figure 1.4. H_2O_2 is a relatively stable ROS, and thus, it can serve as an indicator molecule alerting to the presence of more reactive radical species.[24]

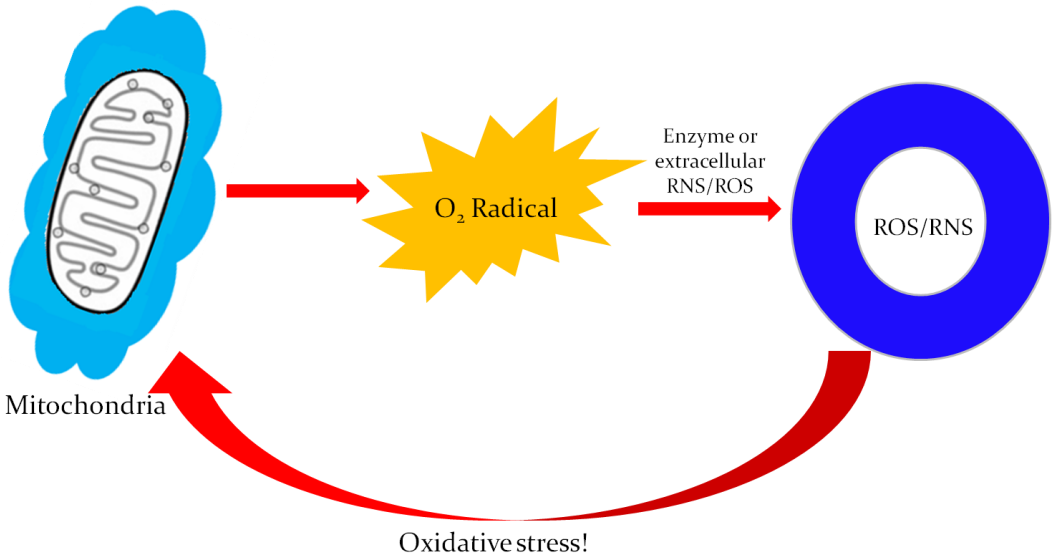

Figure 1.4: **Mitochondrial Dysfunction and Oxidative Stress.** Respiring mitochondria generate ROS such as superoxide anion, which is then converted to other ROS/RNS. When there is an imbalance in the ROS/RNS present, oxidative stress occurs and causes mitochondrial dysfunction.

Several other mechanisms contribute to the pathogenesis of PD. The ways in which protein aggregation and misfolding contribute to the disease are widely controversial. This is in part due to the post-mortem tissue analysis of patients with PD in which the presence of protein aggregates known as Lewy bodies varies from significant to non-existent.[17] It has been hypothesized that the misfolding and improper distribution and release of the protein α-synuclein is key to the pathogenesis of PD.[25] Aggregation of misfolded proteins can also lead to protein sequestration of components that are vital to cell survival. Oxidative stress can contribute to protein aggregation and misfolding as well. [7, 26]

1.7 Treatment for Parkinson's Disease

Currently there is no cure for PD and the treatment for PD has remained relatively unchanged since the 1960's.[7] Treatment for is aimed at restoring the DA deficit created by the loss of DA neurons. This is accomplished by L-DOPA therapy. Though this does not restore DA neurons, it can restore dopaminergic tone. DA is not capable of crossing the blood-brain-barrier due to its size, polarity and limited interactions with the protein responsible for transport across the blood-brain-barrier, large amino acid transporter (LAT). However, L-DOPA the precursor to DA is actively moved across the blood-brain-barrier by LAT. Thus, PD therapy is aimed at increasing DA levels in the brain by increasing the amount of L-DOPA present for the conversion to DA. To prevent the conversion of L-DOPA to DA peripherally (before crossing the blood-brain-barrier), an AADC inhibitor is given with L-DOPA. Furthermore, MAO inhibitors, COMT inhibitors can be coupled with L-DOPA to further increase DA levels in the brain.

L-DOPA has successfully been used to treat the symptoms of PD by increasing DA available for release in the remaining neurons. However, the therapeutic window for L-DOPA therapy narrows and its efficacy wanes over time. As the disease progresses, the efficacy of L-DOPA therapy is hindered by the development of L-DOPA induced dyskinesia. This is characterized by involuntary movements often involving the arms and legs as well as the trunk.[27,28] The cause of L-DOPA induced dyskinesia remains unknown, though studies have implicated oxidative stress as a contributing factor to L-DOPA induced dyskinesia.[29] In order to make progress in understanding the molecular mechanisms that underlie basic brain function as well as dysfunction in PD, we must be able to quantitatively measure neurochemicals in real-time.

1.8 Current Techniques to Monitor Chemicals in the Brain

Communication between neurons is complex as it involves a complex interplay of chemical and electrical signals. Neurotransmitters and other chemicals present in the brain rapidly fluctuate with sub-second temporal resolution to elicit a specific biological or physiological response. Because the brain is a complex mixture of a vast number of chemicals and hundreds of billions of living cells, understanding the chemical mechanisms that underlie brain function is a difficult task.

The most commonly used method for studying neurotransmitters in the brain is a sampling technique known as microdialysis. A microdialysis probe is designed to mimic a blood capillary, consisting of a shaft (1-4 mm in diameter) with a semi-permeable membrane at its tip, which is connected to inlet and outlet tubing. This probe is surgically placed into a brain region of interest and artificial cerebrospinal fluid (aCSF), is perfused at a low flow rate

of approximately 0.1 – 5 μL·min^{-1}. Small solutes present in the brain can cross the semi-permeable membrane by passive diffusion. The solution leaving the probe (dialysate) is collected at timed intervals, separated and quantified. Typically this is accomplished with high performance liquid chromatography (HPLC), a technique that is well-suited for this type of analysis.[30] Figure 1.5 illustrates a typical microdialysis probe that is inserted into the brain to monitor neurotransmitters. However, sample collection requires multiple minutes—this is not commensurate with the timescale of neuronal signaling (sub-second). Furthermore, the size of the microdialysis probe (1-4 mm) precludes measurements in discrete brain regions.[30]

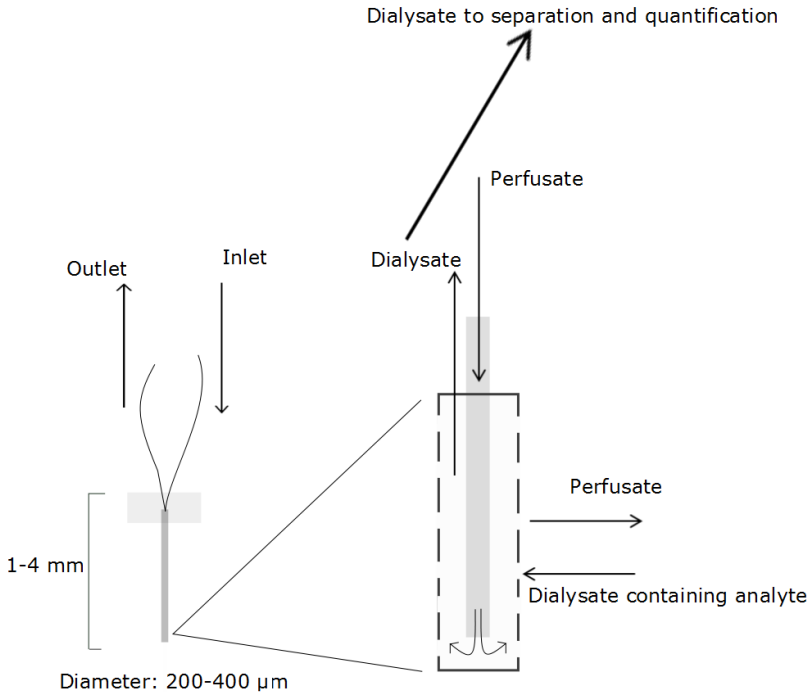

Figure 1.5 Microdialysis Probe. A microdialysis probe is generally 1-4 mm in length and 200-400 μm in diameter. The inset shows the probe/tissue interface. Perfusate is flowed down an inlet tube to a semi-permeable membrane the perfusate interacts with the analyte and diffuses back into the membrane as dialysate that then is collected for separation and quantification through an outlet tube.

1.9 Electrochemical Techniques to Monitor Chemicals in the Brain

Electrochemistry is well-suited for the quantitative analysis of neurotransmission because real-time measurements can be made using microelectrodes that impart minimal tissue damage. Electrochemical techniques to monitor neurotransmitters include amperometry and voltammetry.[31] Amperometry is commonly used to study neurotransmitters in biological systems. In this technique a single potential is applied to an electrode, and any molecules that exhibit redox activity at that potential contribute to the signal. A variation of this technique is chronoamperometry in which a potential step is repeatedly applied.[32] However; these approaches do not provide selectivity to discriminate between species detected at the electrode surface. Fast-scan cyclic voltammetry (FSCV) is an electrochemical technique that combines selectivity with sensitivity.[33] FSCV is a potential sweep method in which the potential applied to the electrode is varied linearly with time. Specifically, FSCV employs sweep rates that are much faster than those applied to conventional electrodes (greater than 100 $V \cdot s^{-1}$) and have been used up to 10^6 $V \cdot s^{-1}$ when coupled to ultramicroelectrodes.[31, 34] A triangular waveform is typically used. This consists of a holding potential that is varied linearly up to a maximum potential, also called the switching potential, and then returned to the holding potential. This is then repeated at a specific rate, typically 10 Hz. The applied waveform is chosen based on the oxidation or reduction properties of the analyte of interest, and can be tailored to monitor specific molecules depending on the properties of the system.

FSCV is most often coupled with carbon-fiber microelectrodes. Carbon materials are used as sensing surfaces because they operate in a wide potential window and are chemically

inert, allowing for the detection of many types of analytes.[31] They are compatible in biological systems and resist biofouling that can distort voltammetric peaks and alter electron transfer kinetics much better than metal-based electrodes. These carbon sensors are also inexpensive and easy to fabricate. Furthermore, the small size of carbon-fiber microelectrodes enables high speed measurements, and the small current results in a smaller ohmic drop that may alter electrochemical measurements. This eliminates the requirement for an auxiliary electrode.[32] The use of carbon-fiber microelectrodes with FSCV also creates a unique situation in which the carbon sensing surface is regenerated through the application of the waveform, with each scan oxygen-containing functional groups are regenerated and help maintain the sensitivity of an electrode when the applied potential is scanned up to 1.3 V vs. Ag/AgCl.[35] An image of a typical carbon-fiber microelectrode used with FSCV is shown in Figure 1.6. The dimensions of a typical carbon-fiber microelectrode used with FSCV are 5-7 μm in diameter and the exposed carbon fiber is 100-300 μm in length.[31]

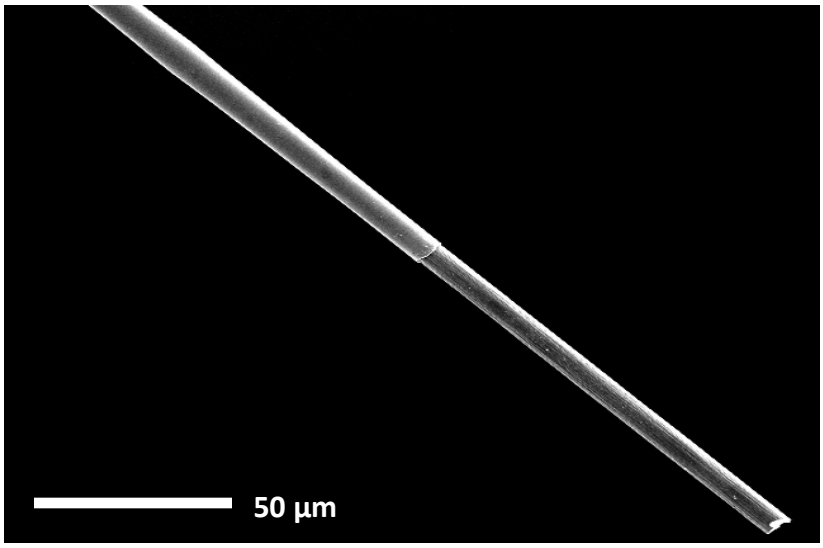

Figure 1.6 SEM Image of a Carbon-Fiber Microelectrode. A carbon-fiber microelectrode is composed of an exposed sensing surface, generally cut with a surgical scalpel to a length of 100-300 µm. The diameter of the carbon-fiber is 5-7 µm.

1.10 Detecting Dopamine with FSCV in Living Brain Tissue

The use of FSCV at carbon-fiber microelectrodes is a powerful tool to monitor rapidly fluctuating molecules such as neurotransmitters in living brain tissue in real-time.[36] The rapid sweep rate associated with FSCV provides sub-second temporal resolution necessary to observe dynamic changes in neurotransmitters. Additionally, the small size of the probe imparts minimal tissue damage and provides the necessary spatial resolution to distinguish between discrete brain regions that can vary significantly.

The most commonly used waveform for monitoring DA has a negative holding potential of -0.4 V vs. Ag/AgCl during the ~90 msec between scans. Thus, positively-charged DA molecules pre-concentrate at the electrode surface. The potential is then linearly

swept at a rate of 400 V·s^{-1} up to +1.3 V and back to -0.4 V a rate of 10 Hz.[37] Figure 1.7 illustrates the established waveform used for the detection of DA. A large background or capacitative current is generated when recording in a buffer solution or brain tissue. This background current is a result of non-faradaic processes occurring at the electrode surface. When an analyte of interest is oxidized or reduced at the electrode surface an additional faradaic current is generated. Since the non-faradaic background current is stable over time it can be subtracted to reveal the smaller faradaic current. As the potential is ramped upward on the anodic scan toward the switching potential DA is oxidized (0.6 V vs. Ag/AgCl.) to dopamine-o-quinone in a two-electron transfer process. On the cathodic return scan, dopamine-o-quinone (-0.2 V vs. /AgCl.) is reduced back to DA. When the background subtracted faradaic current is plotted with respect to applied voltage a unique voltammogram for DA is generated (Figure 1.8).

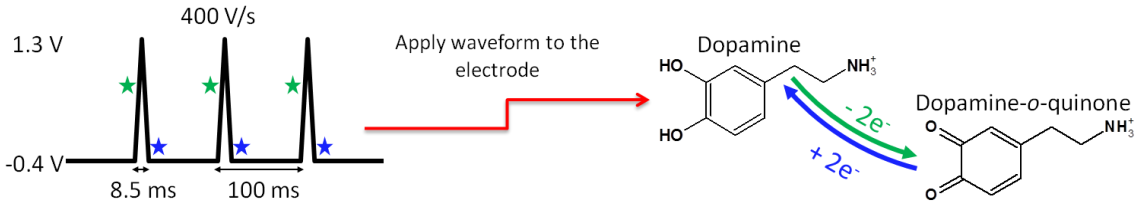

Figure 1.7 Fast-Scan Cyclic Voltammetry. With FSCV a triangular waveform is applied to the carbon-fiber microelectrode ranging from -0.4 V to 1.3 V vs. Ag/AgCl. On the anodic scan DA is oxidized to dopamine-o-quinone. It is reduced back to DA on the cathodic scan. The flow of electrons is measured as current that is proportional to the concentration of DA at the electrode surface.

The faradaic current can be converted to concentration during post-calibration enabling quantification of real-time DA fluctuations. Therefore this technique provides both qualitative and quantitative data in brain tissue. The process of background subtraction reveals the cyclic voltammogram (current vs. potential) used to identify DA is shown in Figure 1.8. Data is generally collected at a frequency of 10 Hz. Therefore for a 30 second file we generate 30,000 data points. In order to better understand this large volume of data at a glance we plot the linear voltammograms with respect to time in a color plot.

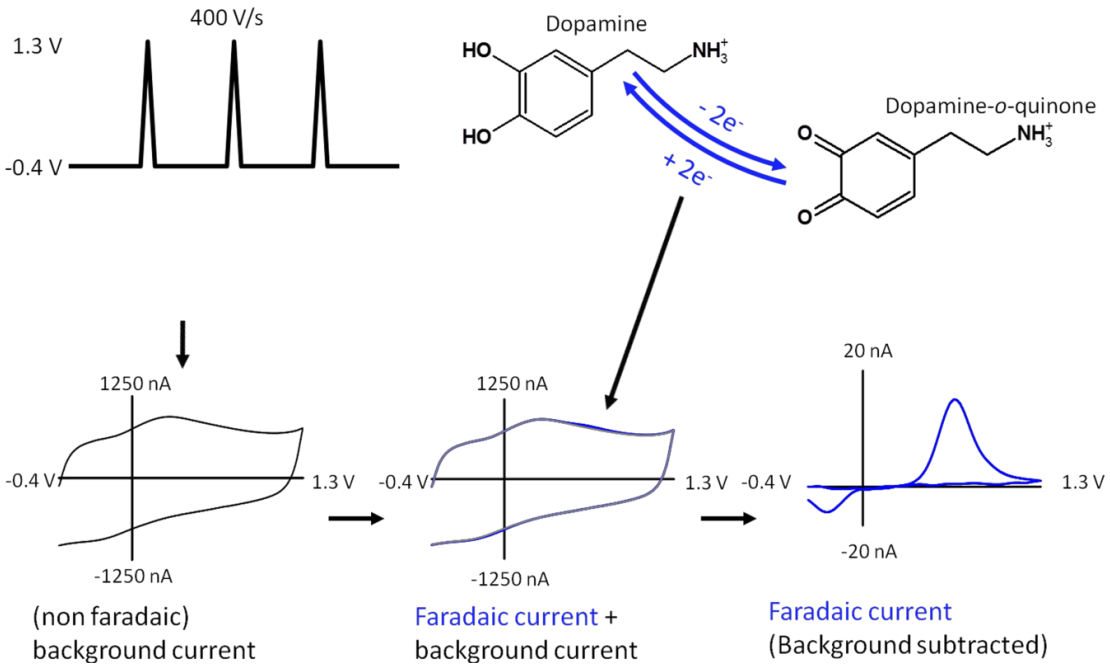

Figure 1.8 Background Subtracted FSCV. Applying the waveform in a buffer solution or in living tissue generates a large background, non-faradaic current. Upon introduction of the analyte, the current slightly changes. A background subtracted cyclic voltammogram unique to DA, is obtained from subtracting the cyclic voltammogram of the faradaic and background current from the background

The applied voltage is plotted as the ordinate, time is plotted as the abscissa and changes in current are plotted using a color representation on the z-axis. This allows visualization of data collected at all of the potentials. As different analytes have distinct voltammograms, multiple chemical species can be visually discriminated in the data at any given point. Figure 1.9 demonstrates how a colorplot for DA is obtained.

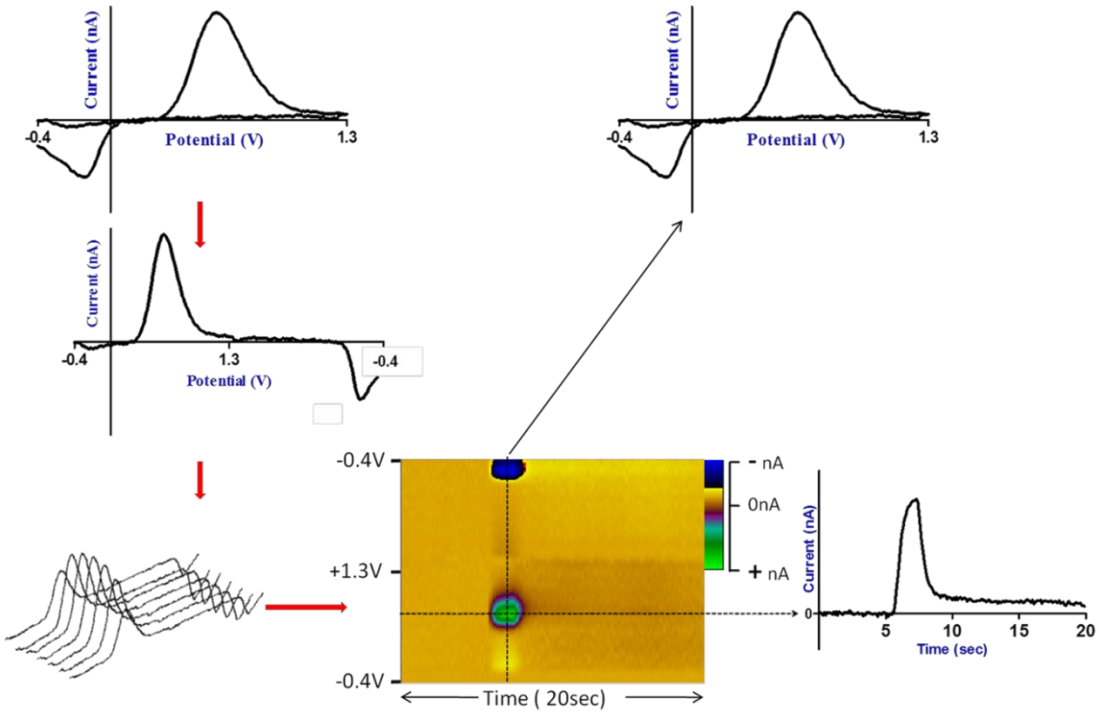

Figure 1.9 Displaying the Data. Each voltammogram obtained is unfolded at the switching potential and concatenated. The data is presented as a three dimensional colorplot with potential on the y-axis, time on the x-axis and the current plotted on the z-axis as false color.

1.11 Chemical Modification of Carbon-Fiber Microelectrodes

Although FSCV at carbon-fiber microelectrodes is a powerful technique for monitoring molecules in neuroscience, there are interferents in the brain that can limit the applicability of the technique. Some molecules, including serotonin and a variety of neuropeptides, have been shown to polymerize at the electrode surface decreasing electrode sensitivity and reproducibility to the analyte of interest.[38] For these reasons, many permselective membranes have been coated onto carbon-fiber microelectrodes to improve performance.

Nafion-coated carbon-fiber microelectrodes have been used extensively to increase the sensitivity of cationic analytes and expel anionic interfering species that oxidize or reduce in a similar potential window. Nafion is a perfluorinated cation-exchange polymer developed by Walther Grot of DuPont in the 1960s. The polymer is synthesized from the Teflon monomer, perfluorinated alkyl vinyl ether, and sulfonyl acid that is treated with sodium hydroxide to yield sulfonate groups that are terminally functionalized on the polymer.[39] The structure is shown in Figure 1.10. The terminal sulfonate group is key to the ion-exchange properties of Nafion.

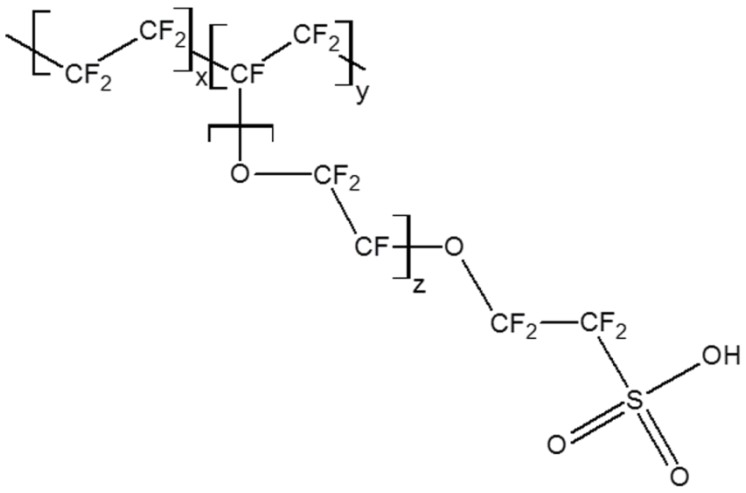

Figure 1.10 Structure of Nafion. The perfluorinated polymer, Nafion, is made from a Teflon backbone. The polymer was first synthesized by Walther Grot of DuPont in the 1960s. The terminal sulfonate group allows Nafion to be selectively permeable to cationic macromolecules present in brain tissue and has been used to exclude anionic interferences in electrochemical studies.

The use of Nafion to detect cationic neurotransmitters in the central nervous system (CNS) at carbon electrodes was first described by Ralph Adams in 1985.[40] Since then, the polymer has been widely used and has been shown to be beneficial in detecting neurotransmitters with primary amines (serotonin, DA, and norepinephrine) while excluding interfering anionic species (ascorbic acid) and biogenic amine metabolites.[40] Furthermore, the use of Nafion can increase the sensitivity of electrodes to these cations without significantly slowing the time response on the electrode.[41]

1.12 Conclusion

Understanding the chemical dynamics underlying brain function and dysfunction remains one of the greatest modern scientific challenges. Advances in technology have provided us with the necessary tools to uncover the chemical dynamics underlying brain

function. Despite these advances, some molecules have been elusive and some studies inconclusive. A complete understanding of the brain and neurodegenerative disease states relies exclusively in the continued advancement of investigative tools including advances in neuroanalytical techniques. Electrochemical techniques, FSCV in particular, have provided us with the ability to monitor neuroactive molecules in real-time. The unique properties of FSCV and future advancements in neuroanalytical tools and neuroscience from continued research in the field will lend themselves to unprecedented discoveries that can help us understand neurodegenerative disease states like PD, and form the foundation for which new therapies can be developed.

REFERENCES CHAPTER 1

1. Bear, M. C., BW; Paradiso, MA, *Neuroscience: Exploring the Brain (3rd ed)*. Third ed.; Lippincott, Williams & Wilkins: Baltimor, MD, 2007.

2. Albanese, A.; Altavista, M. C.; Rossi, P., Organization of central nervous system dopaminergic pathways. *J Neural Transm Suppl* **1986,** *22*, 3-17.

3. Kopin, I. J., Catecholamine metabolism: basic aspects and clinical significance. *Pharmacol Rev* **1985,** *37* (4), 333-64.

4. Elsworth, J. D.; Roth, R. H., Dopamine synthesis, uptake, metabolism, and receptors: relevance to gene therapy of Parkinson's disease. *Exp Neurol* **1997,** *144* (1), 4-9.

5. Elmore, S., Apoptosis: a review of programmed cell death. *Toxicol Pathol* **2007,** *35* (4), 495-516.

6. Kanduc, D.; Mittelman, A.; Serpico, R.; Sinigaglia, E.; Sinha, A. A.; Natale, C.; Santacroce, R.; Di Corcia, M. G.; Lucchese, A.; Dini, L.; Pani, P.; Santacroce, S.; Simone, S.; Bucci, R.; Farber, E., Cell death: apoptosis versus necrosis (review). *Int J Oncol* **2002,** *21* (1), 165-70.

7. Dexter, D. T.; Jenner, P., Parkinson disease: from pathology to molecular disease mechanisms. *Free Radic Biol Med* **2013**.

8. Van Den Eeden, S. K.; Tanner, C. M.; Bernstein, A. L.; Fross, R. D.; Leimpeter, A.; Bloch, D. A.; Nelson, L. M., Incidence of Parkinson's disease: variation by age, gender, and race/ethnicity. *Am J Epidemiol* **2003,** *157* (11), 1015-22.

9. Jankovic, J., Parkinson's disease: clinical features and diagnosis. *J Neurol Neurosurg Psychiatry* **2008,** *79* (4), 368-76.

10. Parkinson, J., *An Essay on the Shaking Palsy*. Whittingham and Rowland: London, 1817.

11. Goetz, C. G., The history of Parkinson's disease: early clinical descriptions and neurological therapies. *Cold Spring Harb Perspect Med* **2011,** *1* (1), a008862.

12. Dauer, W.; Przedborski, S., Parkinson's disease: mechanisms and models. *Neuron* **2003,** *39* (6), 889-909.

13. Hirsch, E.; Graybiel, A. M.; Agid, Y. A., Melanized dopaminergic neurons are differentially susceptible to degeneration in Parkinson's disease. *Nature* **1988,** *334* (6180), 345-8.

14. Beninger, R. J., The role of dopamine in locomotor activity and learning. *Brain Res* **1983,** *287* (2), 173-96.

15. Jellinger, K. A., Pathology of Parkinson's disease. Changes other than the nigrostriatal pathway. *Mol Chem Neuropathol* **1991,** *14* (3), 153-97.

16. Bergstrom, B. P.; Garris, P. A., "Passive stabilization" of striatal extracellular dopamine across the lesion spectrum encompassing the presymptomatic phase of Parkinson's disease: a voltammetric study in the 6-OHDA-lesioned rat. *J Neurochem* **2003,** *87* (5), 1224-36.

17. Jenner, P., Oxidative stress in Parkinson's disease. *Ann Neurol* **2003,** *53 Suppl 3*, S26-36; discussion S36-8.

18. Tieu, K.; Ischiropoulos, H.; Przedborski, S., Nitric oxide and reactive oxygen species in Parkinson's disease. *IUBMB Life* **2003,** *55* (6), 329-35.

19. Schober, A., Classic toxin-induced animal models of Parkinson's disease: 6-OHDA and MPTP. *Cell Tissue Res* **2004,** *318* (1), 215-24.

20. Przedborski, S.; Ischiropoulos, H., Reactive oxygen and nitrogen species: weapons of neuronal destruction in models of Parkinson's disease. *Antioxid Redox Signal* **2005,** *7* (5-6), 685-93.

21. Hirsch, E. C.; Breidert, T.; Rousselet, E.; Hunot, S.; Hartmann, A.; Michel, P. P., The role of glial reaction and inflammation in Parkinson's disease. *Ann N Y Acad Sci* **2003,** *991*, 214-28.

22. Mizuno, Y.; Ohta, S.; Tanaka, M.; Takamiya, S.; Suzuki, K.; Sato, T.; Oya, H.; Ozawa, T.; Kagawa, Y., Deficiencies in complex I subunits of the respiratory chain in Parkinson's disease. *Biochem Biophys Res Commun* **1989,** *163* (3), 1450-5.

23. Schapira, A. H.; Cooper, J. M.; Dexter, D.; Clark, J. B.; Jenner, P.; Marsden, C. D., Mitochondrial complex I deficiency in Parkinson's disease. *J Neurochem* **1990,** *54* (3), 823-7.

24. Bao, L.; Avshalumov, M. V.; Patel, J. C.; Lee, C. R.; Miller, E. W.; Chang, C. J.; Rice, M. E., Mitochondria are the source of hydrogen peroxide for dynamic brain-cell signaling. *J Neurosci* **2009,** *29* (28), 9002-10.

25. Lucking, C. B.; Brice, A., Alpha-synuclein and Parkinson's disease. *Cell Mol Life Sci* **2000,** *57* (13-14), 1894-908.

26. Rubinsztein, D. C., The roles of intracellular protein-degradation pathways in neurodegeneration. *Nature* **2006,** *443* (7113), 780-6.

27. Obeso, J. A.; Olanow, C. W.; Nutt, J. G., Levodopa motor complications in Parkinson's disease. *Trends Neurosci* **2000,** *23* (10 Suppl), S2-7.

28. Mouradian, M. M.; Heuser, I. J.; Baronti, F.; Fabbrini, G.; Juncos, J. L.; Chase, T. N., Pathogenesis of dyskinesias in Parkinson's disease. *Ann Neurol* **1989,** *25* (5), 523-6.

29. Jenner, P., Molecular mechanisms of L-DOPA-induced dyskinesia. *Nat Rev Neurosci* **2008,** *9* (9), 665-77.

30. Chefer, V. I.; Thompson, A. C.; Zapata, A.; Shippenberg, T. S., Overview of brain microdialysis. *Curr Protoc Neurosci* **2009,** *Chapter 7*, Unit7 1.

31. Robinson, D. L.; Hermans, A.; Seipel, A. T.; Wightman, R. M., Monitoring rapid chemical communication in the brain. *Chem Rev* **2008,** *108* (7), 2554-84.

32. Bard, A. J.; Faulkner, L. R., *Electrochemical methods : fundamentals and applications*. 2nd ed.; Wiley: New York, 2001; p xxi, 833 p.

33. Millar, J.; Stamford, J. A.; Kruk, Z. L.; Wightman, R. M., Electrochemical, pharmacological and electrophysiological evidence of rapid dopamine release and removal in the rat caudate nucleus following electrical stimulation of the median forebrain bundle. *Eur J Pharmacol* **1985,** *109* (3), 341-8.

34. Amatore, C.; Maisonhaute, E., When voltammetry reaches nanoseconds. *Anal Chem* **2005,** *77* (15), 303A-311A.

35. Roberts, J. G.; Moody, B. P.; McCarty, G. S.; Sombers, L. A., Specific oxygen-containing functional groups on the carbon surface underlie an enhanced sensitivity to dopamine at electrochemically pretreated carbon fiber microelectrodes. *Langmuir* **2010,** *26* (11), 9116-22.

36. Roberts, J. G.; Lugo-Morales, L. Z.; Loziuk, P. L.; Sombers, L. A., Real-time chemical measurements of dopamine release in the brain. *Methods Mol Biol* **2013,** *964*, 275-94.

37. Heien, M. L.; Phillips, P. E.; Stuber, G. D.; Seipel, A. T.; Wightman, R. M., Overoxidation of carbon-fiber microelectrodes enhances dopamine adsorption and increases sensitivity. *Analyst* **2003,** *128* (12), 1413-9.

38. Hashemi, P.; Dankoski, E. C.; Petrovic, J.; Keithley, R. B.; Wightman, R. M., Voltammetric detection of 5-hydroxytryptamine release in the rat brain. *Anal Chem* **2009,** *81* (22), 9462-71.

39. Grot, W., *Fluorinated ionomers*. William Andrew Pub.: Norwich, NY, 2008; p xii, 238 p.

40. Gerhardt, G. A.; Oke, A. F.; Nagy, G.; Moghaddam, B.; Adams, R. N., Nafion-coated electrodes with high selectivity for CNS electrochemistry. *Brain Res* **1984,** *290* (2), 390-5.

41. Kristensen, E. W.; Kuhr, W. G.; Wightman, R. M., Temporal characterization of perfluorinated ion exchange coated microvoltammetric electrodes for in vivo use. *Anal Chem* **1987,** *59* (14), 1752-7.

CHAPTER 2

Electrochemical Detection of Nitric Oxide

2.1 Introduction to Reactive Nitrogen Species

RNS are highly reactive nitrogen and oxygen containing molecules that are known to contribute to nitroxidative and oxidative stress.[1,2,3] In particular, NO, a highly reactive, free radical RNS, is involved in a diverse array of biological functions including signal transduction in the nervous system as a gaseous neurotransmitter.[4,5] NO is endogenously produced within a cell from the reduction of L-arginine through a family of enzymes known as NOS and can quickly and easily diffuse across cell membranes.[6,7]

NO has been implicated in the onset and progression of various neurodegenerative diseases including PD by contributing to oxidative stress. Though NO has been shown to be cytoprotective, evidence suggests that derivatives of NO such as peroxynitrite and nitrogen dioxide contribute to oxidative stress resulting in both cell dysfunction and cell death.[1,2] Due to the role that NO and its derivatives play in nitroxidative and oxidative stress, understanding the various functions of NO in the brain and the extent to which this central molecule contributes to oxidative and nitroxidative stress is crucial to understanding the mechanisms underlying neurodegenerative disease states such as PD.

2.2 Measuring Nitric Oxide in Biological Systems

The detection and quantification of NO in biological systems is generally accomplished in one of three ways, by means of spectrophotometric techniques, indicator species, and electrochemical techniques.[8] Spectrophotometric techniques provide the capacity to eliminate interferences and are capable of measuring NO more directly than

indicator techniques. However, spectrophotometric analyses often require derivitization of NO to induce a signal, such as with chemiluminesence and fluorescence methods. In these types of analyses, derivitization of NO induces spectrophotometric signals that cannot be easily quenched, thus signals cannot be isolated limiting the selectivity of this technique for NO. Indicator techniques such as the Griess assay are commonly used as this is the most cost effective method of detecting NO. The Griess assay requires a secondary molecule, in this case nitrite, which can only be detected once bound to sulphanilic acid producing a color change to estimate initial concentrations of NO in biological systems.[9] It was recently shown that the Griess assay is significantly less effective in various physiological buffers used to quantify NO than both chemiluminesence and electrochemical techiques.[10]

The electroactive properties of NO make electrochemical techniques an inherently viable method for the quantification and identification of NO. Electrochemical sensors can be made from a variety of materials and tailored to provide discrete spatial resolution in samples such as single cells and brain nuclei.[11] NO diffuses rapidly, approximately 3300 $\mu m^2 \cdot s^{-1}$, and readily reacts with many species often found in physiological buffers, including oxygen and carbon dioxide.[12,13] Electrochemical techniques provide the ability to make rapid chemical measurements of NO in living tissue and biological media providing the necessary temporal resolution to quantify a rapidly fleeting analyte such as NO.

2.3 Electrochemical Measurements of Nitric Oxide

The oxidation of NO is a three electron process that proceeds in multiple steps as an electrochemical chemical electrochemical (ECE) reaction. The oxidation of NO is typically observed between +0.6 and +0.9 V versus Ag/AgCl.[14] In the initial electrochemical step NO

is converted to NO^+, in a single electron transfer step. NO^+ then reacts in an immediate chemical step. In the third and final electrochemical step, nitrate and hydrogen ions are produced. The reaction scheme for the oxidation of NO is shown in equations 2.1-2.3.[8]

$$NO \rightarrow NO^+ + e^- \quad (2.1)$$

$$NO^+ + OH^- \rightarrow HNO_2 \quad (2.2)$$

$$HNO_2 + H_2O \rightarrow NO_3^- + 2e^- + 3H^+ \quad (2.3)$$

The majority of electrochemical sensors used in biological media have utilized the electrochemical oxidation of NO; however, some electrochemical approaches rely on monitoring its reduction. [8] This occurs in a single electron transfer step between - 0.5 and -1.4 V versus Ag/AgCl. The electron transfer of the reduction of NO is presented in equation 4.[15] Although the electrochemical reduction of NO proceeds in a single step process, various obstacles complicate detection. The reduction potentials of NO (-0.5 and -1.4 V vs. Ag/AgCl) and oxygen (-1.4 V vs. Ag/AgCl) are sufficiently close that oxygen may interfere with the detection of NO.[15, 16] Furthermore, other chemical species present in biological media make NO sensors operating via electroreduction particularly prone to the irreversible adsorption of molecules in solution (also called fouling).[8, 11] These are also sensitive to pH shifts, such that observing dynamic fluctuations of NO are obscured.[11]

$$2NO + 2e^- \rightarrow N_2O_2^- \quad (2.4)$$

There are also a number of interferents that could mask the detection of NO via oxidation, including nitrite (produced in the second electron transfer step of the oxidation of NO), dopamine (+0.6 V vs. Ag/AgCl),uric acid (+0.3 V vs. Ag/AgCl) and ascorbic acid (+0.4 V vs. Ag/AgCl) which are electroactive in similar potential windows.[8, 11,17] However, polymeric permselective membranes, such as Nafion have been successfully used to improve selectivity.

To date, the overwhelming majority of sensors for the detection of NO in biological systems rely on amperometry.[18] Though this technique provides a wide dynamic range (pM-mM), amperometric sensors lack selectivity, thus any species present in the solution that oxidizes or reduces at a similar potential contributes to the signal.[11] In comparison, the use of FSCV provides sub-second temporal resolution, micron spatial resolution as well as high sensitivity and selectivity for analytes of interest. Cyclic voltammograms provide a unique chemical signature, enabling discrimination of specific analytes in complex biological mixtures. This is particularly important due to the vast number of chemical components and present in the brain. This work demonstrates the foundation and preliminary work of quantifying and characterizing RNS, specifically NO, using FSCV at carbon-fiber microelectrodes.

2.4 Materials and Methods

2.4.1 Chemicals

All chemicals were purchased from Sigma-Aldrich (Milwaukee, WI) and used as received unless otherwise noted. Phosphate buffered saline (PBS) solution adjusted to pH

7.40 was used in all flow injection analysis experiments. Aqueous solutions were prepared using doubly distilled deionized water (Milli-Q Millipore, Billerica, MA).

2.4.2 Electrode Fabrication

Carbon-fiber microelectrodes were constructed in house. A single T-650 carbon fiber (Cytec Industries, West Patterson, NJ), 7 μm in diameter, is aspirated through a 0.4 mm inner diameter borosilicate glass capillary (A-M systems, Inc., Sequim, WA) and tapered with a heat puller (Narishige, Japan) to create a tight seal around the exposed carbon fiber. Each electrode was then cut to approximately 100 μm under a microscope (Zeiss Primostar) using a surgical scalpel. Electrodes were then inspected for cracks in the seal and for the appropriate length. A metal lead coated in conductive silver paint (GC Electronics, Silver Print II, Rockford, IL) was then inserted into the electrode and secured with heat shrink tubing.

2.4.3 Data Acquisition

All *in vitro* studies were performed using a flow injection apparatus. For all experiments a triangular waveform from -0.4 to +1.4 V vs. Ag/AgCl was applied at a scan rate of 400 $V \cdot s^{-1}$ at a frequency of 10 Hz. The instrument used to apply the potential to the electrochemical cell and for signal transduction was custom built (United World Dominion, Mebane, NC). Waveform output was accomplished using TarHeel CV software (UNC-Chapel Hill, Chapel Hill, NC) with a DAC/ADC card (NI 6251 M). Triggering and synchronization of electrochemical experiments with flow injection was accomplished using a NI 6711 card. Background subtraction, averaging and filtering was controlled using a 4-pole Bessel Filter at 2.5 kHz.

2.4.4 Flow Injection

Carbon-fiber microelectrodes were placed in a custom-built electrochemical cell (NCSU Chemistry Machine Shop) using a micromanipulator (World Precision Instruments, Inc. Sarasota, FL). Buffer was continuously supplied at a flow rate of 1 $mL \cdot min^{-1}$ across the working and reference electrode using a syringe pump (NE 300, New Era Pump Systems, Inc., Farmingdale, NY). Analytes were introduced to the microelectrode surface in 5 second bolus injections via a six-port HPLC valve attached to an air actuator by means of a digital pneumatic solenoid valve kit (Valco Instruments, Houston, TX). The flow injection apparatus was housed in a home-built Faraday cage. Unless otherwise specified, all experiments were performed at room temperature.

2.4.5 Preparation of Nafion-Coated Electrodes

Bare carbon-fiber microelectrodes were electrochemically pre-treated by applying the waveform for 10 minutes at 60 Hz and subsequently for 10 minutes at 10 Hz. Electrodes were then initially tested for ascorbic acid sensitivity, rinsed with doubly deionized water, and cleaned for 30 minutes in filtered isopropyl alcohol. A solution of 5 % Nafion in methanol (Ion Power DuPont 10521 Nafion Solution, New Castle, DE) was electro-deposited onto the electrode by applying a potential of +1.0 V versus Ag/AgCl for 30 seconds forming a membrane. Electrodes were then dried in an oven at 70°C for ten minutes to ensure that the methanol was evaporated. Each Nafion-coated electrode was then tested for sensitivity to ascorbic acid, to verify the integrity of the Nafion membrane. Only those exhibiting less than 25 % of the initial response to ascorbic acid were used in subsequent experiments.

2.4.6 Nitric Oxide Sample Preparation

All NO stock solutions were graciously supplied courtesy of Dr. Mark Schoenfisch in the department of Chemistry at UNC-Chapel Hill. Solutions of filtered PBS at pH 7.40 were placed on ice in centrifuge tubes and capped with a rubber septum. A stainless steel cylinder containing saturated potassium hydroxide was used to scavenge any oxygen present in the argon used to purge the solution and the NO used to prepare the stock solution. PBS solutions were bubbled with argon for approximately 30 minutes, followed by NO gas for 20 min. The resulting stock solution contained 1.9 mM NO.[7] Standard solutions (10-38 μM) were freshly prepared using the saturated NO solution in argon-bubbled PBS (pH 7.40). All standard solutions were prepared in an oxygen-free atmosphere (courtesy of Dr. Reza Ghiladi at NCSU).

2.4.7 Statistics

For all studies, n refers to the number of electrodes. Statistical significance was designated at $P < 0.05$ using a one-tailed Student's t-test. All graphical and statistical analyses were accomplished using GraphPad Prism 5 (GraphPad Software, Inc., La Jolla, CA).

2.5 Results and Discussion

2.5.1 Nitric Oxide Cyclic Voltammetry

For all NO studies, data was collected in an *in vitro* flow injection apparatus. The potential applied to the electrode was ramped linearly from -0.4 to 1.4 V versus Ag/AgCl at 400 $V \cdot s^{-1}$ and at a frequency of 10 Hz to oxidize NO in solution. A representative voltammogram following the introduction of a 5 s bolus injection of 10 μM NO solution is presented in Figure 2.1 A. Two oxidative peaks are present in the voltammogram. The first

peak occurs at approximately 1.35 V versus Ag/AgCl on the anodic scan. This may possibly correspond to the first electrochemical step generating NO^+. A second oxidative peak appears near the switching potential. These two oxidative peaks are also present in the representative colorplot as shown in Figure 2.1 B.

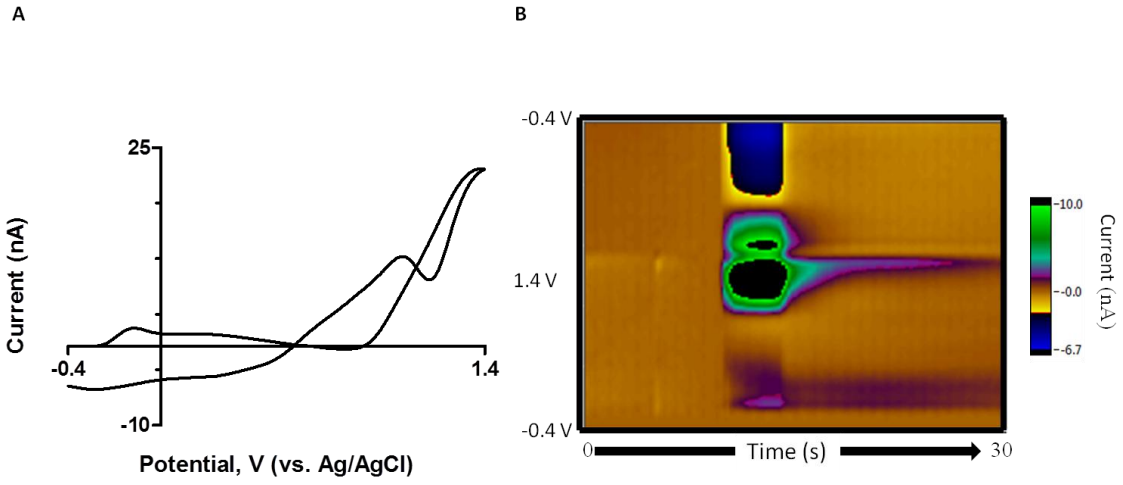

Figure 2.1 Nitric Oxide Representative Voltammogram and Colorplot. (A) Representative cyclic voltammogram for the oxidation of NO. Two oxidative peaks are present. The first occurs on the anodic scan at 1.35 V vs. Ag/AgCl. The second peak occurs on the cathodic scan at 1.0 v vs. Ag/AgCl. Some cathodic current is evident at approximately 0.28 V vs. Ag/AgCl on the return scan. (B) Corresponding colorplot, both oxidative peaks are present in the colorplot

The final electrochemical step in the oxidation of NO produces nitrate and hydrogen ions. If detected at our electrode, this would result in a pH shift in the data. The cathodic current evident in the NO voltammograms is likely due to an acidic pH shift. For

comparison, representative voltammograms and the corresponding color plot for an acidic pH shift (7.30 or ΔpH = -0.1) are shown in Figure 2.2 A-B.

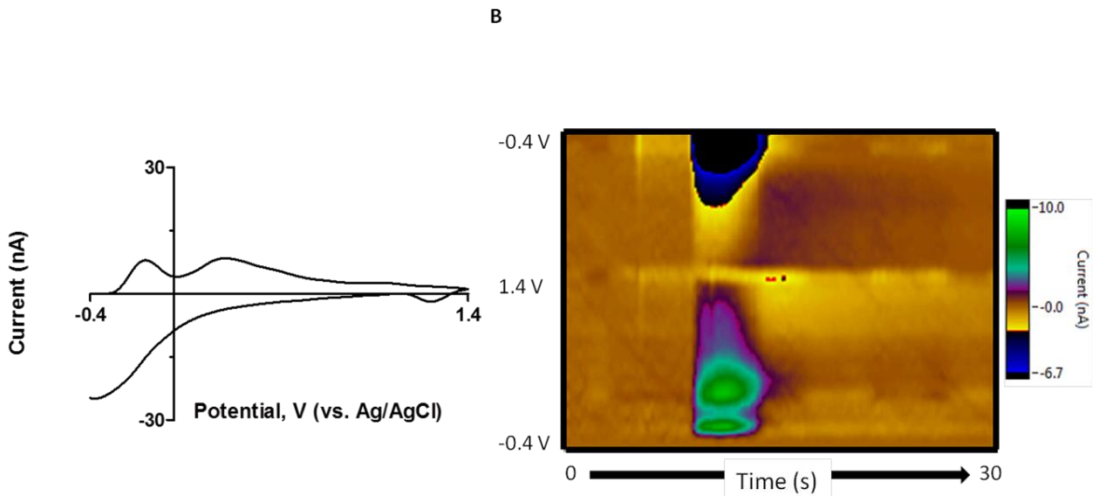

Figure 2.2: **Acidic pH Shift Representative Voltammogram and Colorplot**. (A) Representative cyclic voltammogram for an acidic pH shift of 7.30 or ΔpH = -0.1 (B) Corresponding colorplot

The relationship between current and NO concentration was characterized (10-38 μM). Figure 2.3 A demonstrates representative cyclic voltammograms for increasing concentrations of NO and the corresponding calibration curve is shown in Figure 2.3 B (*n* = 1). The current increases with increasing concentrations of NO. However, the response between electrodes was highly variable, as seen in Figure 2.3 C-D. The maximum current is expected to correspond to the highest concentration of NO; however, this was not always the case and this contributes to the variability inherent to Figure 2.3 A-D. The variability can be attributed to several possibilities. All dilutions prepared from the stock NO solution (1.9 mM) were prepared in PBS bubbled with argon. The argon used to purge the PBS of oxygen

did not include passage through a stainless steel cylinder containing saturated potassium hydroxide as described in the preparation of calibration and stock solutions of NO.[7] Although gases used in this study were high purity, traces of oxygen and other oxidant species may have been present in the argon, differentially affecting each solution. A second possibility is excessive aeration of the samples. Although samples were prepared in an oxygen-free atmosphere, the flow injection apparatus was not housed in an oxygen-free atmosphere. Samples were drawn from vials via 5 mL syringes and injected into the six-port HPLC valve. Any aeration of the samples may have changed the concentration of NO present in solution, affecting the voltammetric response. The variability in the electrochemistry of NO was then exacerbated upon serial dilution of the samples.

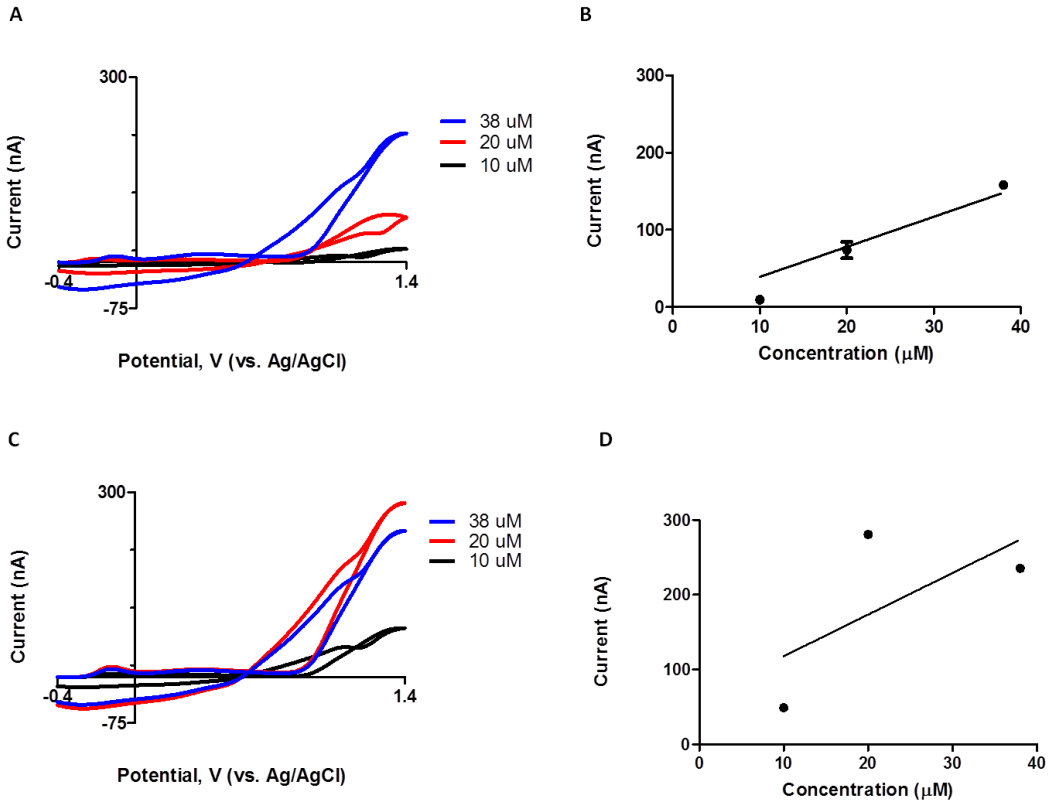

Figure 2.3: **Current Response to Varying Concentrations of NO**. (A) Representative voltammograms for n=1 electrode. (B) Corresponding calibration curve showing increasing current with increasing concentration. (C) Representative voltammograms for n=1 electrode. Variability in current response to varying concentrations of NO is also seen here. (D) Corresponding calibration curve demonstrating variability between electrodes assessed on the same day.

2.5.2 Variability in Nitric Oxide Electrochemistry

The variability in the electrochemistry of NO was also evident between batches of stock solution. As seen in Figure 2.4, voltammograms collected from different stock solutions in different months and years lack reproducibility. Again, this may be attributed to non-ideal argon bubbling or aeration of samples. The voltammogram in Figure 2.4 for the

February injection appears to be an acidic pH shift. This can be compared with the voltammogram from Figure 2.2 A.

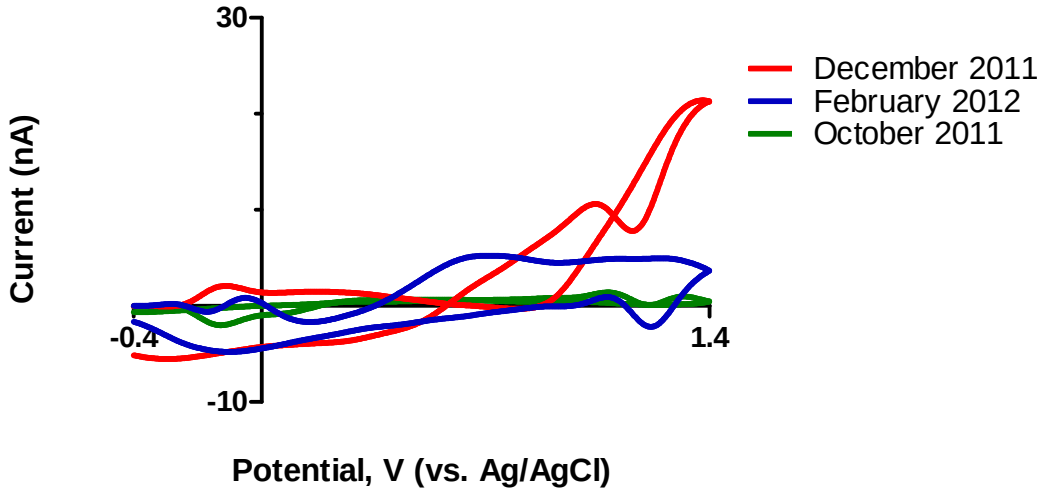

Figure 2.4 Variability in NO Voltammetry between Batches. The voltammograms for a 10 μM bolus injection of NO varied from solution to solution.

2.5.3 Nitric Oxide Detection at Nafion-Coated Electrodes

Due to the variability exhibited in preliminary electrochemical experiments, Nafion was used to coat the carbon-fiber microelectrodes. Recall that Nafion is a cation exchange polymer that has been shown to increase sensitivity to NO and expel interfering anionic species. [17, 19] Figure 2.5 A depicts representative voltammograms for varying concentrations of NO collected at Nafion-coated carbon-fiber microelectrodes (n = 2). As expected, with increasing concentrations of NO, the current increases as seen in Figure 2.5 B.

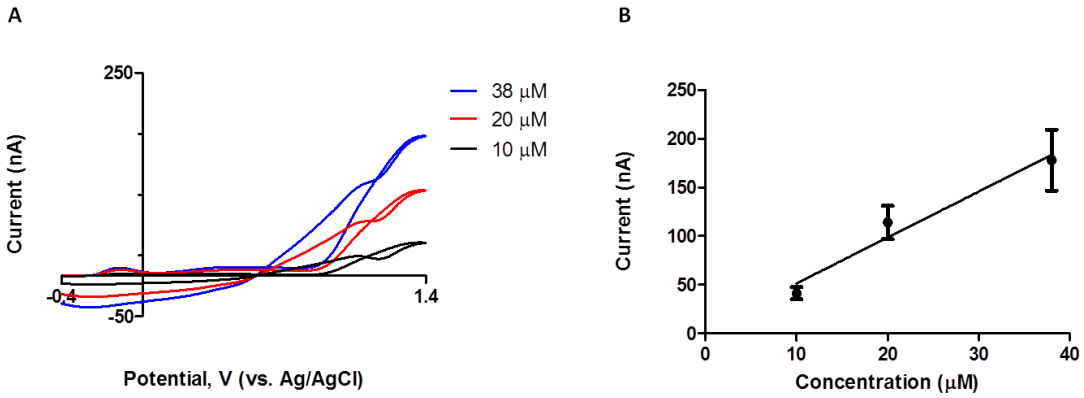

Figure 2.5 FSCV of Nitric Oxide at Nafion-Coated Electrodes (A) Cyclic voltammograms of increasing concentrations of NO for n = 2 electrodes. (B) Increasing current with increasing concentrations of NO at Nafion-coated electrodes, the current increases with increasing concentration.

A direct comparison of bare versus Nafion-coated carbon-fiber electrodes is shown in Figure 2.6 A-C. For each concentration, the current response at Nafion-coated electrodes is greater than that of the bare electrodes. The Nafion-coated electrode current response is significantly greater than that of bare electrodes for both the 10 and 20 µM solutions (Figure 2.6 D , $P < 0.05$, $n = 2$, Student's t-test).

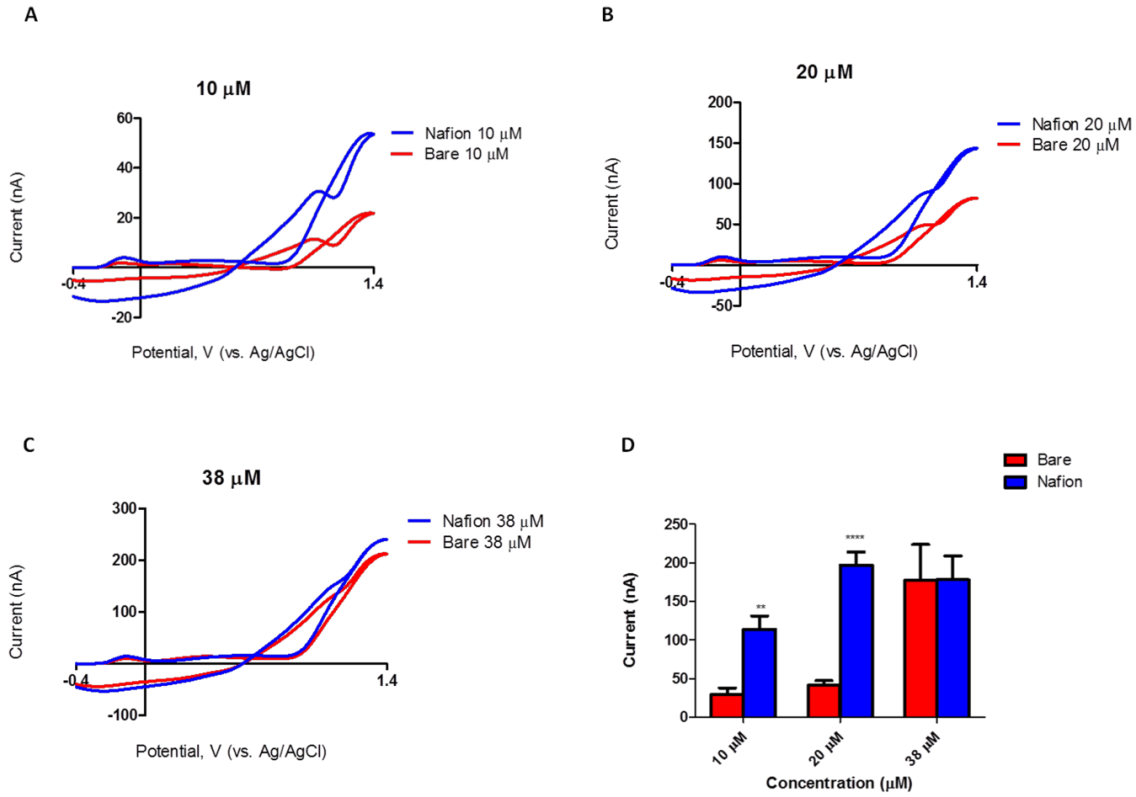

Figure 2.6 Comparison of Bare and Nafion-Coated Electrodes (A-C) Representative voltammograms of the current response of bare carbon and Nafion -coated electrodes to NO. (D) Comparison of bare and Nafion –coated electrodes at various concentrations using a one-tailed Student's t-test (significance $P < 0.05$, n=2). The current was significantly increased at Nafion-coated electrodes for both 10 and 20 µM NO. There was no difference in the current at bare and Nafion-coated electrodes for 38 µM NO.

The current response of the highest concentration of NO solution (38 µM) at Nafion-coated electrodes was not significantly different than the current response of bare electrodes. When using a bare electrode, some samples produce more current for the 20 µM solution of NO than the 38 µM solution of NO (Figure 2.3). This may have contributed to the lack of significance at the highest concentration. Nafion is a cation exchange polymer, therefore a

Nafion membrane at a carbon-fiber microelectrode surface has the capacity to exclude interfering anionic species that may interfere with the detection of an analyte of interest. Nitrite produced during the oxidation of NO may interfere with the detection .[8] The enhancement in signal seen with Nafion-coated carbon-fiber microelectrodes may in part be due to expelling nitrite present at the electrode surface.

2.6 Conclusion

The data presented in this study provide a foundation for the quantification and characterization of NO with FSCV at carbon-fiber microelectrodes. A unique voltammetric signature for NO was obtained and found to contain two oxidation peaks. The first oxidation peak is present at approximately 1.35 V versus Ag/AgCl, and the second is evident near the switching potential. A reduction peak was also present at approximately 0.28 V versus Ag/AgCl. This could be attributed to an acidic pH shift due to nitrate and hydrogen ions generated in the final electrochemical step of the oxidation of NO (equation 2.3). There was significant variability in the data, possibly due to the introduction of oxygen to NO solutions. The use of Nafion as a permselective membrane significantly enhanced the current in response to concentration at calibration standards of 10 and 20 μM NO solutions. In order to optimize and validate the detection of NO with FSCV, further studies should investigate various parameters to discriminate NO from other ROS and RNS, and to better define the chemical transformations at the electrode surface. The linear dynamic range for NO detected with FSCV should be assessed. Although the concentrations evaluated in this study produced a signal, the concentrations may have surpassed the linear dynamic range for NO detected with FSCV. This could be evaluated by assessing the current response of lower

concentrations of NO at Nafion-coated carbon-fiber microelectrodes if aeration and improper bubbling of the samples can be controlled. The switching potential should be optimized to produce well-resolved peaks. Although the waveform employed in this study was sufficient to oxidize NO, the oxidation peaks are poorly resolved. Varying the scan rate would also help to determine if the chemical step, defined in equation 2 is taking place. At 400 $V \cdot s^{-1}$, we may be outrunning this reaction. A slower scan rate on the order of 0.1-10 $V \cdot s^{1}$ would allow us to investigate this further. However, maintaining a fast scan rate is necessary for detection in live tissue, as these chemical species are short-lived. Selectivity versus common interferents must be assessed. Next, the approach should be validated in live tissue using a controlled condition, such as application of exogenous NO to a brain slice. Finally, validation by pharmacological manipulation is necessary. The use of a drug to manipulate the signal in a predictable manner will build confidence in the approach.

REFERENCES CHAPTER 2

1. Przedborski, S.; Dawson, T. M., The role of nitric oxide in Parkinson's disease. *Methods Mol Med* **2001,** *62*, 113-36.

2. Tieu, K.; Ischiropoulos, H.; Przedborski, S., Nitric oxide and reactive oxygen species in Parkinson's disease. *IUBMB Life* **2003,** *55* (6), 329-35.

3. Moilanen, E.; Vapaatalo, H., Nitric oxide in inflammation and immune response. *Ann Med* **1995,** *27* (3), 359-67.

4. Ignarro, L. J.; Buga, G. M.; Wood, K. S.; Byrns, R. E.; Chaudhuri, G., Endothelium-derived relaxing factor produced and released from artery and vein is nitric oxide. *Proc Natl Acad Sci U S A* **1987,** *84* (24), 9265-9.

5. Rand, M. J.; Li, C. G., Nitric oxide as a neurotransmitter in peripheral nerves: nature of transmitter and mechanism of transmission. *Annu Rev Physiol* **1995,** *57*, 659-82.

6. Habib, S.; Ali, A., Biochemistry of nitric oxide. *Indian J Clin Biochem* **2011,** *26* (1), 3-17.

7. Davies, I. R.; Zhang, X., Nitric oxide selective electrodes. *Methods Enzymol* **2008,** *436*, 63-95.

8. Privett, B. J.; Shin, J. H.; Schoenfisch, M. H., Electrochemical nitric oxide sensors for physiological measurements. *Chem Soc Rev* **2010,** *39* (6), 1925-35.

9. Griess, P., On a New Series of Bodies in Which Nitrogen is Substituted for Hydrogen. *Phil. Trans. R. Soc. Lond.* **1864,** *154*.

10. Hunter, R. A.; Storm, W. L.; Coneski, P. N.; Schoenfisch, M. H., Inaccuracies of nitric oxide measurement methods in biological media. *Anal Chem* **2013,** *85* (3), 1957-63.

11. Hetrick, E. M.; Schoenfisch, M. H., Analytical chemistry of nitric oxide. *Annu Rev Anal Chem (Palo Alto Calif)* **2009,** *2*, 409-33.

12. Malinski, T.; Taha, Z.; Grunfeld, S.; Patton, S.; Kapturczak, M.; Tomboulian, P., Diffusion of nitric oxide in the aorta wall monitored in situ by porphyrinic microsensors. *Biochem Biophys Res Commun* **1993,** *193* (3), 1076-82.

13. Zacharia, I. G.; Deen, W. M., Diffusivity and solubility of nitric oxide in water and saline. *Ann Biomed Eng* **2005,** *33* (2), 214-22.

14. Brunet, A.; Pailleret, A.; Devynck, M. A.; Devynck, J.; Bedioui, F., Electrochemical sensing of nitric oxide for biological systems: methodological approach and new insights in examining interfering compounds. *Talanta* **2003,** *61* (1), 53-9.

15. Bartberger, M. D.; Liu, W.; Ford, E.; Miranda, K. M.; Switzer, C.; Fukuto, J. M.; Farmer, P. J.; Wink, D. A.; Houk, K. N., The reduction potential of nitric oxide (NO) and its importance to NO biochemistry. *Proc Natl Acad Sci U S A* **2002,** *99* (17), 10958-63.

16. Venton, B. J.; Michael, D. J.; Wightman, R. M., Correlation of local changes in extracellular oxygen and pH that accompany dopaminergic terminal activity in the rat caudate-putamen. *J Neurochem* **2003,** *84* (2), 373-81.

17. Robinson, D. L.; Hermans, A.; Seipel, A. T.; Wightman, R. M., Monitoring rapid chemical communication in the brain. *Chem Rev* **2008,** *108* (7), 2554-84.

18. Amatore, C.; Arbault, S.; Bouton, C.; Drapier, J. C.; Ghandour, H.; Koh, A. C., Real-time amperometric analysis of reactive oxygen and nitrogen species released by single immunostimulated macrophages. *Chembiochem* **2008,** *9* (9), 1472-80.

19. Gerhardt, G. A.; Oke, A. F.; Nagy, G.; Moghaddam, B.; Adams, R. N., Nafion-coated electrodes with high selectivity for CNS electrochemistry. *Brain Res* **1984,** *290* (2), 390-5.

CHAPTER 3

Investigating the Effect of L-DOPA Treatment at Microelectrodes with Fast-Scan Cyclic Voltammetry in Brain Slice Tissue

3.1 Introduction

PD is a neurodegenerative disease in which DA neurons that project from the SN to the dorsal striatum selectively degenerate.[1,2] Clinical manifestations of this disease are characterized by motor deficits such as rigidity, resting tremor, bradykinesia and akinesia.[3,4] Typically, symptoms do not present until 60-85% of DA neurons are destroyed.[5] There is currently no cure for PD and the treatment for PD has remained unchanged since the 1960s.[6] The goal of PD pharmacotherapy is aimed at decreasing the DA deficit by restoring dopaminergic tone through increasing the available L-DOPA , the precursor to DA. Despite the effectiveness of L-DOPA therapy to treat symptoms of PD, serious complications are associated with prolonged treatment with L-DOPA.[7] Thus creating the need to understand the molecular mechanisms underlying DA potentiation with L-DOPA therapy in PD.

The effects of L-DOPA on DA release have been studied in both intact and Parkinsonian-like rodent models using doses of L-DOPA ranging from 6 $mg \cdot kg^{-1}$ to 250 $mg \cdot kg^{-1}$ and have demonstrated that L-DOPA can significantly increase DA levels in the brain .[8,9,10,11,12] Furthermore, significant increases in electrically-evoked DA release have been elicited in single cells and brain slice studies with concentrations of L-DOPA ranging from 60-100 μM.[13,14,15] This work aims to investigate the effect of L-DOPA on DA dynamics at a more clinically relevant dose of L-DOPA in a rat brain slice. Brain slice tissue preparations can be used to study the effects of L-DOPA treatment on DA release

since many biological functions are preserved in the brain slice.[16] Specifically, striatal brain slices preserve the terminals of neurons originating in the SN, and these can be pharmacologically manipulated with ease, and without the confounding effects of afferent projections to the region. The rates of DA release and reuptake can be quantified by comparing data collected in response to an electrical stimulation using the electrochemical form of the Michaelis-Menten equation. This model is well characterized and takes advantage of the unparalleled temporal and spatial resolution of FSCV to quantify the maximum DA release and the rate of its reuptake into the presynaptic terminal by way of the DAT. [11,12,17] The electrochemical form of the Michaelis-Menten equation is presented in equation 3.1.

$$\frac{d[DA]}{dt} = [DA]_p f - \frac{V_{max}}{\left(\frac{K_m}{[DA]}+1\right)} \qquad (3.1)$$

DA release is a function of the DA evoked per stimulus pulse ($[DA]_p$) and the frequency (*f*) at which the stimulus is delivered. Reuptake is defined in the second term of the equation. V_{max} is the maximum reuptake rate of DA achieved by the DAT. K_m is the Michaelis constant; a measure of the affinity of DA for the DAT, the value of K_m in the dorsal striatum is accepted to be 0.16 μM.[18, 19] The instantaneous [DA] is found by determining the difference between release and reuptake. The model is capable of predicting changes in V_{max} and K_m following pharmacological manipulation.[20] Changes in V_{max} and K_m will differentially alter the slope of the curve shown in Figure 3.1.

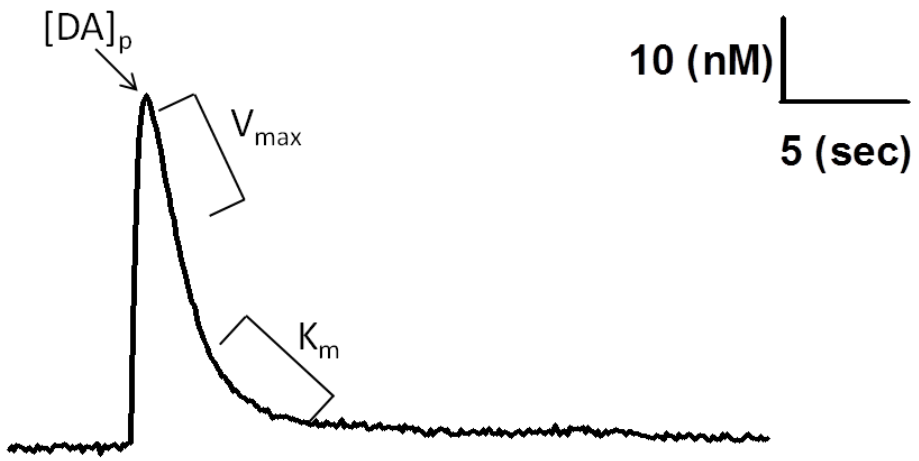

Figure 3.1 Modeling Michaelis-Menten Kinetics with FSCV. $[DA]_p$ is the DA released per stimulus pulse as a function of the frequency of the stimulus pulse, V_{max} corresponds to the maximum uptake rate of DA. K_m is the Michaelis constant for DA at the DAT, and a value of 0.16 μM is accepted for the dorsal striatum.

DA neurons in the brain fire in both tonic and phasic modes.[21] Tonic DA firing occurs at frequencies less than 20 Hz and is constant over longer periods of time. Phasic DA firing, or burst firing, occurs at greater than 20 Hz. Phasic firing events elicit prominent DA 'transients' in the striatum of intact rats.[22] The burst firing of DA neurons is highly implicated in motivated behavior, and in well-trained animals striatal DA transients occur time-locked to the delivery of cues that predict reward availability.[23, 24, 25] Thus, there is broad interest in understanding phasic DA firing because these events, and the DA that is released, may be a target in pharmacotherapies for drug abuse and addiction. This work examined the effects of L-DOPA on the dynamics of DA released in response to single pulse electrical stimulations, as well as to artificial 'bursts' in healthy control animals.

Understanding the parameters that govern the rates of DA release and reuptake in response to L-DOPA treatment in this control group will provide a framework enabling us to interpret the effects of this drug on Parkinsonian animals with compromised DA systems.

3.2 Materials and Methods

3.2.1 Chemicals

All chemicals were purchased from Sigma-Aldrich (Milwaukee, WI) and used as received unless otherwise noted. Phosphate buffered saline (PBS) solution adjusted to pH 7.40 was used in all flow injection analysis experiments. Aqueous solutions were prepared using doubly distilled deionized water (Milli-Q Millipore, Billerica, MA).

3.2.2 Electrode Fabrication

Carbon-fiber microelectrodes were constructed in house. A single T-650 carbon fiber (Cytec Industries, West Patterson, NJ), 7 μm in diameter, is aspirated through a 0.4 mm inner diameter borosilicate glass capillary (A-M systems, Inc., Sequim, WA) and tapered with a heat puller (Narishige, Japan) to create a tight seal around the exposed carbon fiber. Each electrode was then cut to approximately 100 μm under a microscope (Zeiss Primostar) using a surgical scalpel. Electrodes were then inspected for cracks in the seal and for the appropriate length. A metal lead coated in conductive silver paint (GC Electronics, Silver Print II, Rockford, IL) was then inserted into the electrode and secured with heat shrink tubing.

3.2.3 Data Acquisition

All *in vitro* studies were performed using a flow injection apparatus. For all experiments a triangular waveform from -0.4 to +1.3 V vs. Ag/AgCl was applied at a scan

rate of 400 $V \cdot s^{-1}$ at a frequency of 10 Hz. The instrument used to apply the potential to the electrochemical cell and for signal transduction was custom built (United World Dominion, Mebane, NC). Waveform output was accomplished using Demon Voltammetry and Analysis with a DAC/ADC card (NI 6251 M). Triggering and synchronization of electrochemical experiments with flow injection was accomplished using a NI 6711 card.

3.2.4 Flow Injection

Carbon-fiber microelectrodes were placed in a custom built electrochemical cell (NCSU Chemistry Machine Shop) using a micromanipulator (World Precision Instruments, Inc. Sarasota, FL). aCSF buffer was continuously supplied at a flow rate of 1 $mL \cdot min^{-1}$ across the working and reference electrode was accomplished using a syringe pump (NE 300, New Era Pump Systems, Inc., Farmingdale, NY). Analytes were introduced to the microelectrode surface in 5 second bolus injections via a six-port HPLC valve attached to an air actuator by means of a digital pneumatic solenoid valve kit (Valco Instruments, Houston, TX). The flow injection apparatus was housed in a home built Faraday cage. Unless otherwise specified, all experiments were performed at room temperature.

3.2.5 Preparation of Nafion-Coated Electrodes

Bare carbon-fiber microelectrodes were electrochemically pre-treated by applying the waveform for 10 minutes at 60 Hz and subsequently for 10 minutes at 10 Hz. Electrodes were then initially tested for ascorbic acid sensitivity, rinsed with doubly deionized water, and cleaned for 30 minutes in filtered isopropyl alcohol. A solution of 5 % Nafion in methanol (Ion Power DuPont 10521 Nafion Solution, New Castle, DE) was electro-deposited onto the electrode by applying a potential of +1.0 V versus Ag/AgCl for 30 seconds forming

a membrane. Electrodes were then dried in an oven at 70°C for ten minutes to ensure that the methanol was evaporated. Each Nafion-coated electrode was then tested for sensitivity to ascorbic acid; only those exhibiting less than 25 % of the initial response to ascorbic acid were used in experiments.

3.2.6 Animals

Adult male Sprague-Dawley rats (275-300 g) were purchased from Charles River (Raleigh, NC). Rats were housed individually with a 12-h light/dark cycle; food and water were made available *ad libitum*. Animal care and protocols were in compliance with the university IUACUC and NIH guidelines.

3.2.7 Brain Slices

Rats were anesthetized with 1.0 g/mL of urethane, decapitated and their brains were quickly removed and placed in ice-cold, oxygenated (95 % O_2 and 5 % CO_2) 20 mM HEPES acid artificial cerebrospinal fluid (aCSF) containing 124 mM NaCl, 3.7 mM KCl, 26 mM $NaHCO_3$, 2.4 mM $CaCl_2$, 1.3 mM $MgCl_2$, 1.3 mM NaH_2PO_4, 1.3 mM D-glucose and 0.6 mM L-ascorbate adjusted to pH 7.40. Coronal brain slices (400 μm thick) containing the striatum, identified by a rat brain atlas, were prepared using a manual vibrotome (World Precision Instruments, Sarasota FL). Prior to the experiment, slices were kept in oxygenated HEPES acid aCSF. Slices used in the experiment were housed in a locally- constructed brain slice chamber where aCSF was perfused at 1 $mL \cdot min^{-1}$ in aCSF at 34°C for approximately one hour until equilibrated. A borosilicate glass carbon-fiber microelectrode, approximately 100 μm in length and 6-7 μm in diameter (bare or Nafion-coated, depending on the particular experiment), was positioned 75 μm below the surface of the slice in the

dorsal striatum. Electrical stimulation was accomplished using a biphasic stimulation (2 ms each phase) with an amplitude of 400 μA at a bipolar stimulating electrode (FHC, Bowdoin, ME) positioned at a distance of 100-200 μm from the working electrode using a micromanipulator (World Precision Instruments Inc., Sarasota, FL) and an inverted confocal microscope (Nikon Instruments Inc, Melville, NY). The duration of the pulse train for each experiment was kept constant (1 s) and the number of pulses was varied from 20 to 60 (frequencies of 20 and 60 Hz) in addition to a single pulse 400 μA amplitude stimulation. Successive stimulations were separated by 120 sec. Following equilibration, the DA response to electrical stimulation was evaluated at various frequencies and slices were then saturated with either 1 or 50 μM L-3, 4-dihydroxyphenylalanine (L-DOPA) methyl ester for 45 minutes. Electrically-evoked DA was again evaluated for up to 100 minutes past initial saturation with L-DOPA. Finally, fresh aCSF was reintroduced (washout) for 45 minutes, and electrically-evoked dopamine was again evaluated.

3.2.8 Michaelis-Menten Kinetic Analysis

Kinetic analysis was performed using the Michaelis-Menten modeling package in Demon Voltammetry and Analysis Software (Wake Forest University Health Sciences, Winston-Salem, NC). Release ($[DA]_p$)and reuptake kinetics (V_{max}) were determined by evaluating $[DA]_p$ and V_{max} using equation 3.1.[12]

$$\frac{d[DA]}{dt} = [DA]_p f - \frac{V_{max}}{\left(\frac{K_m}{[DA]}+1\right)} \qquad (3.1)$$

[DA] is the instantaneous extracellular concentration of dopamine, *f* is the frequency of the stimulus pulse train, $[DA]_p$ is the dopamine concentration released per pulse, V_{max} is the maximum reuptake rate for dopamine (by the dopamine transporter), and K_m is the Michaelis constant for the affinity of dopamine for the dopamine transporter. Changes in the rates of release and reuptake were determined using the following assumptions of equation 3.1: 1) A fixed quantity of DA is released from pre-synaptic DA neurons for each stimulus pulse 2) uptake is saturable and not finite 3) DA clearance from the extracellular space predominantly occurs via the DAT.[12, 20] K_m was held for the entire experiment at 0.16 μM, as this value has previously been determined for the striatum.[18,19] V_{max} was determined for each experiment. Changes in uptake were attributed to changes in V_{max}.

3.2.9 Statistics

All data is presented as +/- standard error of the mean (SEM). For all *in vitro* studies n refers to the number of electrodes. In all brain slice studies, n represents the number of slices, from different animals. Statistical significance was designated as $P < 0.05$ using one-way ANOVA with Tukey Post-Hoc test. Data is presented as normalized concentration. All graphical and statistical analyses were accomplished using GraphPad Prism 5 (GraphPad Software, Inc., La Jolla, CA).

3.3 Results and Discussion

3.3.1 Background Subtracted Fast-Scan Cyclic Voltammetry of Dopamine

Cyclic voltammograms were collected *in vitro* in the flow injection apparatus (*in vitro* studies) and in striatal brain slices following electrical stimulation. The potential applied to the electrode was varied from a holding potential of -0.4 V to 1.3 V vs. Ag/AgCl and back at

a scan rate of 400 $V \cdot s^{-1}$ every 100 ms depicted in Figure 3.2 A. A large non-faradaic background current was generated as shown in Figure 3.2 B (solid line). The introduction of a 5 s bolus injection of DA (*in vitro)* or electrical stimulation to evoke DA release in the vicinity of the electrode produces faradaic current resulting from the transfer of two electrons in which DA is oxidized to dopamine-o-quinone and reduced back to DA. This current adds to the background non-faradaic current, as shown in Figure 3.2 B (dashed line). Dopamine-specific voltammograms were obtained by subtracting the background current as shown in Figure 3.2 C. The oxidation potential of DA is approximately 0.6 V vs. Ag/AgCl and the reduction peak is observed at approximately -0.2 V vs. Ag/AgCl. Voltammograms collected over a period of 30 seconds are unfolded at the switching potential, concatenated and plotted in three-dimensions with the applied potential as the ordinate, time as the abscissa and current plotted in false color as shown in Figure 3.2 D.

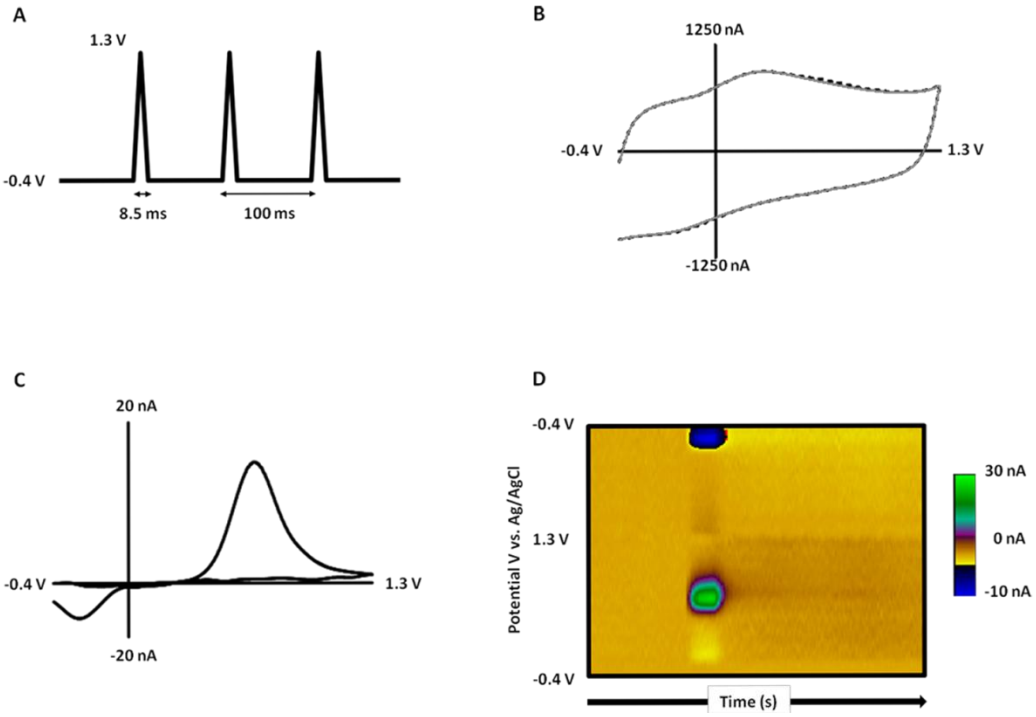

Figure 3.2 Background Subtracted FSCV (A) The applied potential was varied from a holding potential of -0.4 V vs. Ag/AgCl to 1.3 V and back at a scan rate of 400 $V \cdot s^{-1}$ every 100 msec. (B) The scan rate generates a large non-faradaic background current that is stable over time (solid line). Upon the introduction of an analyte of interest an additional faradaic current is evident (dashed line). (C) Background subtracted voltammogram for dopamine. The oxidation is seen at approximately 0.6 V vs. Ag/AgCl, the reduction is seen at approximately -0.2 V vs. Ag/AgCl. (D) Colorplot with voltammograms of DA collected over 30 s. The ordinate is the applied potential, the abscissa is the time and current (nA) is plotted in false color.

3.3.2 In Vitro Assessment of Bare and Nafion-Coated Carbon-Fiber Microelectrodes

L-DOPA can interfere with the detection of DA.[17] The triangular waveform may oxidize L-DOPA and initiate polymerization of the converted quinones at the electrode surface, compromising electrode sensitivity to DA.[2,26] The response to a 1 μM injection of DA in the absence or presence of L-DOPA (1 or 50 μM) was evaluated at bare and Nafion-

coated carbon-fiber microelectrodes in a flow injection apparatus. The experiment consisted of three parts. 1) The current response to a 1 μM injection of dopamine in aCSF was evaluated. 2) The buffer was then altered to contain either 50 μM or 1 μM L-DOPA in aCSF and the current response to a 1 μM injection of dopamine was then re-evaluated. 3) The aCSF was then restored to its original state and the current response to a 1 μM injection of dopamine was evaluated again.

At both bare and Nafion-coated carbon-fiber microelectrodes the presence of 50 μM L-DOPA in the buffer significantly decreased the current response to an injection of 1 μM DA ($P<0.05$, n = 6 and n = 3, respectively), as shown in Figure 3.3 A and B. In both cases re-introduction of clean aCSF did not restore electrode sensitivity, suggesting that there may be fouling of the electrode surface. A lower, more physiologically-relevant concentration of L-DOPA (1 μM) was also evaluated. Interestingly, the presence of 1 μM L-DOPA in the buffer solution did not alter the sensitivity for a 1 μM injection of DA (Figure 3.3 C). However, we did notice that Nafion-coated carbon-fiber microelectrodes exhibited less sensitivity to DA in the washout phase of the experiment ($P< 0.05$, n = 3) as shown in Figure 3.3 D. These results suggest that Nafion may initially prevent fouling of the electrode; however, prolonged exposure or exposure to higher concentrations of L-DOPA may degrade the Nafion membrane and cause the electrode to irreversibly foul.

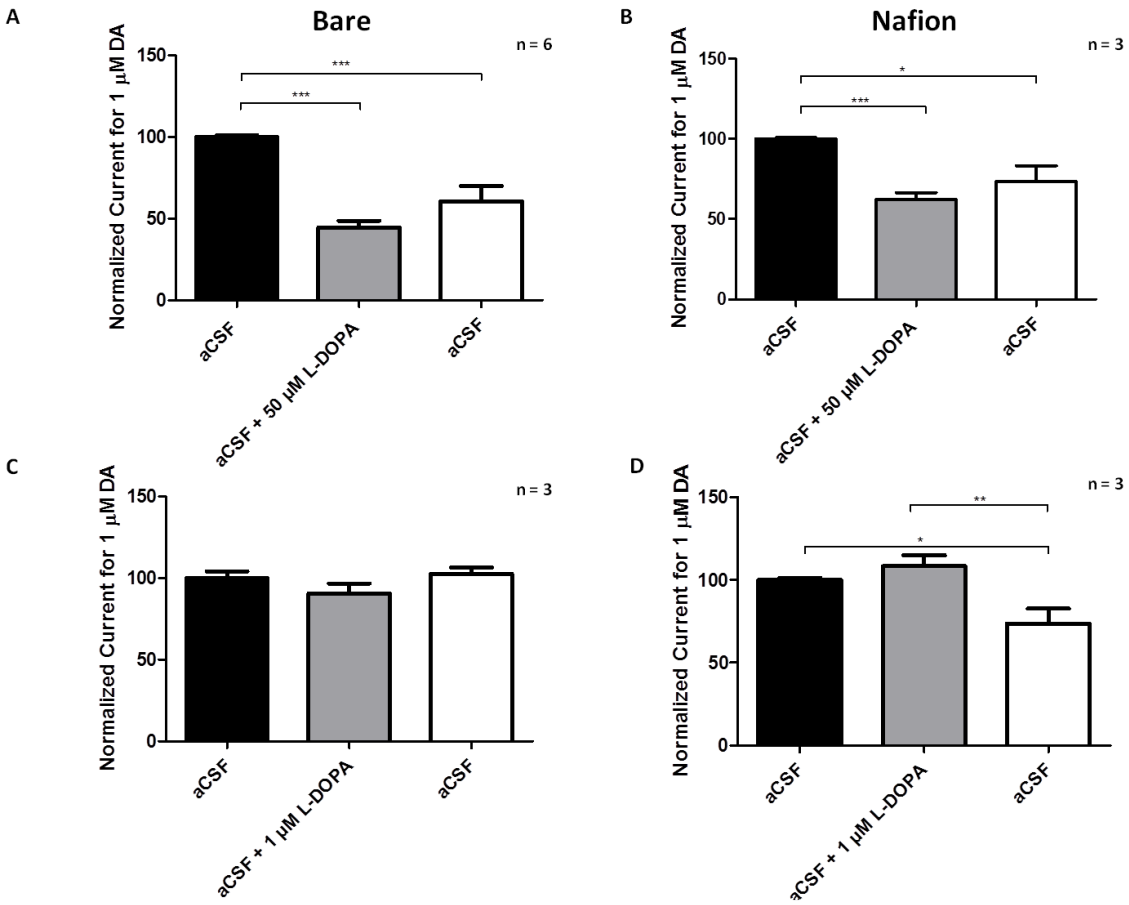

Figure 3.3 *In Vitro* Assessment of Bare and Nafion–Coated Carbon-Fiber Microelectrodes in the Absence and Presence of L-DOPA. Data are expressed at +/- SEM ($P < 0.05$) evaluated with a one-way ANOVA and Tukey post-hoc comparison. Current (nA) is normalized to the pre-drug sensitivity ($nA \cdot \mu M^{-1}$) of DA *in vitro*. When exposed to 50 µM L-DOPA both bare and Nafion coated carbon-fiber microelectrodes sensitivities were significantly decreased ($P < 0.05$, $n = 6$, $n = 3$, respectively). At 1 µM L-DOPA the Nafion-coated carbon-fiber microelectrodes decreased significantly in sensitivity in the washout phase of the experiment ($P < 0.05$, $n = 3$)

3.3.3 Assessing the Effects of L-DOPA on Dopamine Dynamics in Striatal Brain Slices

Electrically-evoked DA release was assessed in coronal brain slices containing the striatum. The working electrode was positioned in the dorsal striatum. The stimulating electrode was positioned approximately 200 µm from the working electrode. Figure 3.4 A

illustrates the location of DA recordings in striatal slices. Representative colorplots and concentration versus time plots of DA release resulting from a single 400 μA stimulation is shown in Figure 3.4 B-E. These data were collected at Nafion-coated carbon-fiber microelectrodes before and after the addition of either 1 or 50 μM L-DOPA. Following 50 μM L-DOPA treatment, the amount of DA release was attenuated as shown in Figure 3.4 B and C. The data collected for each dose with Nafion-coated and bare electrodes were then plotted as several bar graphs to establish the significance of each of the factors (Figure 3.5 A-D). Additionally, the L-DOPA causes DA release to occur over a longer time course. This is likely due to fouling of the electrode surface. Following 1 μM L-DOPA, electrically-evoked DA release remained unchanged as can be observed in the representative colorplots and concentration versus time traces in Figure 3.4 D-E.

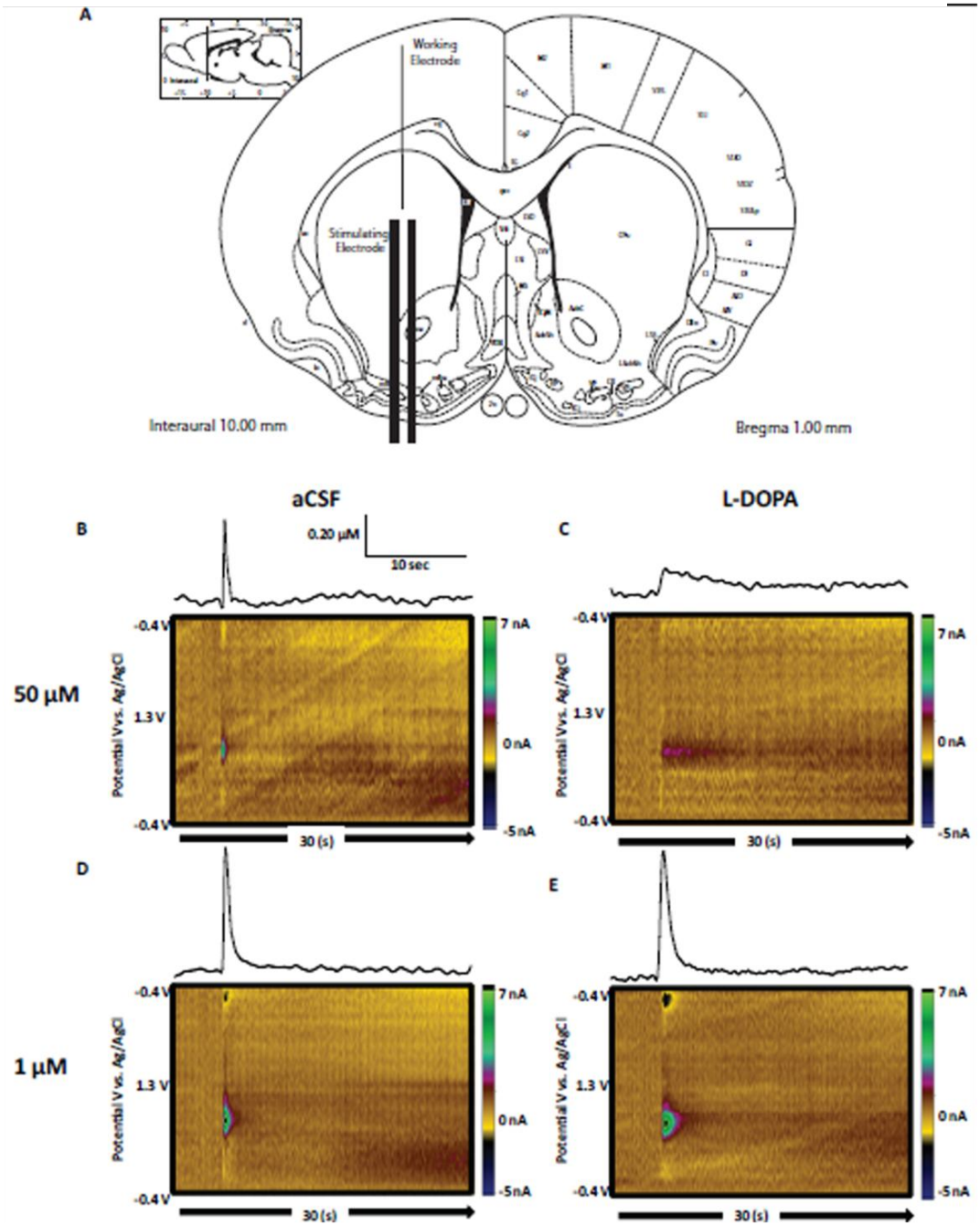

Figure 3.4 Representative Colorplots from Single Pulse Experiments. (A) Diagram of a coronal slice of the rat brain containing the striatum. Electrodes were positioned 75 µm below the tissue in the dorsal striatum. The stimulating electrode was positioned 100-200 µm away.(B-C) Representative colorplots and corresponding concentration vs. time plot of electrically-evoked DA collected at a Nafion-coated carbon-fiber microelectrode before and after 50 µM L-DOPA. DA release appears to decrease after exposure to L-DOPA. (D-E) Representative colorplots and corresponding concentration vs. time plot of electrically-evoked DA before and after 1µM L-DOPA, evoked DA remains unchanged following L-DOPA treatment.

An identical set of experiments were performed at bare carbon-fiber microelectrodes, and the data comparing the two approaches is summarized in Fig 3.5. Here, data is also included from the 'washout' phase of the experiment. At both bare and Nafion-coated electrodes 50 μM L-DOPA significantly reduced the amount of DA detected ($P < 0.05$, $n = 4$) Figure 3.5 A-B. Our *in vitro* experiments suggest that this is likely due to high concentrations of L-DOPA fouling the electrode surface and decreasing electrode sensitivity to DA. A lower dose (1 μM) that did not exhibit this fouling effect *in vitro* was assessed in brain slice tissue. L-DOPA is a DA precursor, and should increase the amount of DA available for release. Because the *in vitro* study at Nafion-coated carbon-fiber microelectrodes suggested that 1 μM L-DOPA did not significantly compromise electrode sensitivity to 1 μM DA, it was expected that1 μM L-DOPA applied to striatal brain slices would potentiate evoked DA. However, Figure 3.5 D shows that evoked DA remained unchanged after treatment with 1 μM L-DOPA. This surprising result may be due to several factors. Treatment with 1 μM L-DOPA may be insufficient to alter electrically-evoked DA release. Alternatively, this treatment may increase the basal levels of DA in the extracellular space; despite the buffer flowing over the slice.[27] Changes in basal DA are not seen with background-subtracted voltammetry, as it is a differential approach. DA release is tightly regulated, and higher basal levels of DA in the extracellular space may activate DA autoreceptors, triggering a negative feedback loop and decreasing evoked DA release. Indeed, a prior chronoamperometric study in anesthetized rats presented this argument to explain data collected in intact animals following a 4 $mg \cdot kg^{-1}$ dose of L-DOPA.[27] Similarly, in a separate study in intact animals, administration of a 5 μM dose of L-DOPA attenuated

DA concentrations.[28] However, it is not possible to directly correlate these studies as the preparations are so different, and the doses are difficult to compare. It is important to note that a single pulse stimulation was used to evoke these data. This models tonic DA firing such that DA release is essentially steady-state, the rate of release and reuptake are balanced and DA release is a function of the stimulus frequency.[11,12] Thus, with a single pulse stimulation, increases in DA following L-DOPA treatment may not be seen.

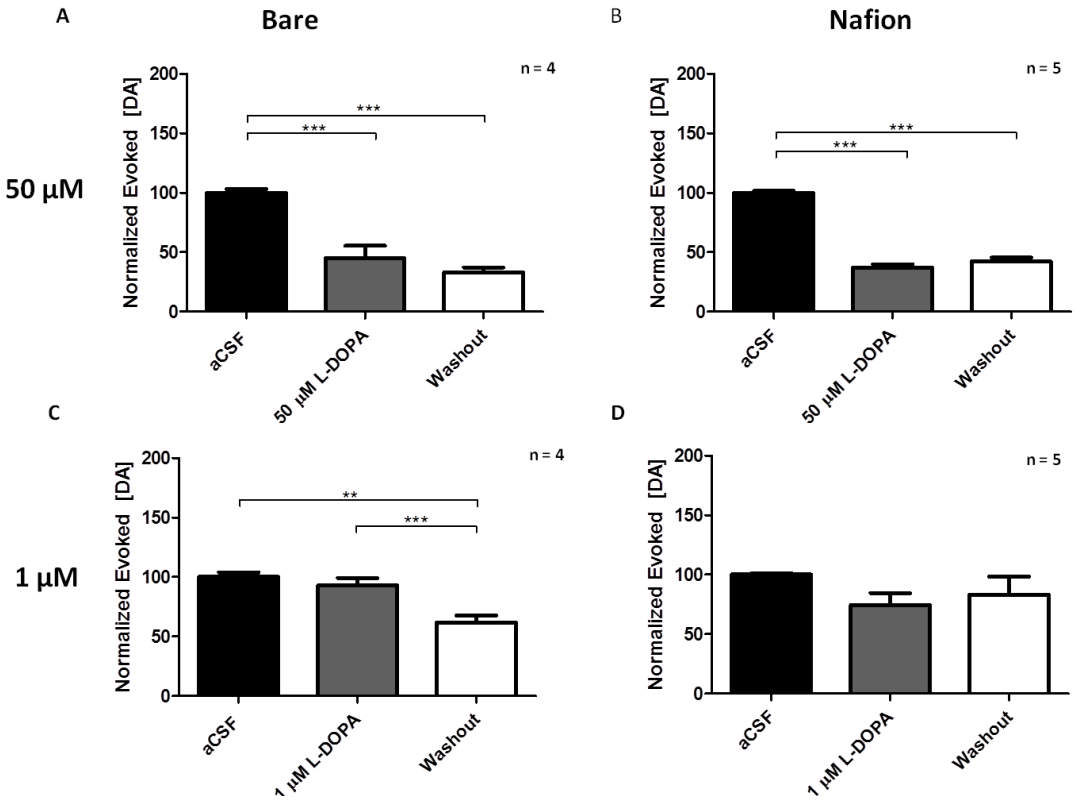

Figure 3.5 Assessment of DA Release in Brain Slice Tissue Treated with L-DOPA. Data are expressed at +/- SEM ($P < 0.05$) evaluated with a one-way ANOVA and Tukey post-hoc comparison. (A-B) Exposure to 50 µM L-DOPA significantly decreased evoked DA at both bare ($P < 0.05$, $n = 4$) and Nafion-coated electrodes ($P < 0.05$, $n = 5$). (C) 1 µM L-DOPA appeared to significantly decrease DA release at bare electrodes in the 'washout' step ($P < 0.05$, $n = 4$. (D) 1 µM L-DOPA did not decrease sensitivity to DA when using Nafion-coated electrodes ($n = 5$)

3.3.4 Electrically-Evoked Dopamine as a Function of Stimulus Frequency and Number of Applied Pulses

In order to address both tonic and phasic neuronal firing, stimulation paradigms have been established whereby the frequency of applied pulses is altered.[12] Those paradigms were adopted in the following set of experiments performed using Nafion-coated carbon-fiber microelectrodes that correspond to the single pulse studies presented above. DA was electrically-evoked at frequencies of 20 (tonic) and 60 (phasic) Hz while maintaining a constant stimulation time of one second. The stimulus paradigm for 20 Hz stimulations consisted of 20 pulses of a 400 μA amplitude. Similarly, 60 Hz stimulations consisted of 60 pulses with an individual pulse amplitude of 400 μA. 50 μM L-DOPA significantly increased the DA release evoked using a 20 Hz, 20 pulse stimulation (Figure 3.6 A, $P<0.05$, $n = 5$). Dopamine remained significantly elevated in the washout even up to and extending beyond 100 minutes after initial saturation with L-DOPA ($P<0.05$, $n =5$). Interestingly, 50 μM L-DOPA did not initially alter the dynamic profile of DA release evoked by the phasic, 60 Hz stimulation. However, the DA release did significantly increase in the washout portion of the experiment ($P< 0.05$, $n =5$) as seen in Figure 3.6 B. The reason for this is unclear. During the washout step of the experiment, aCSF is reintroduced to the brain slice. However, L-DOPA is taken into the slice and converted slowly to DA by enzymes. Although L-DOPA is no longer in the buffer in the washout step it is still in the brain tissue and may have an effect long after the washout.

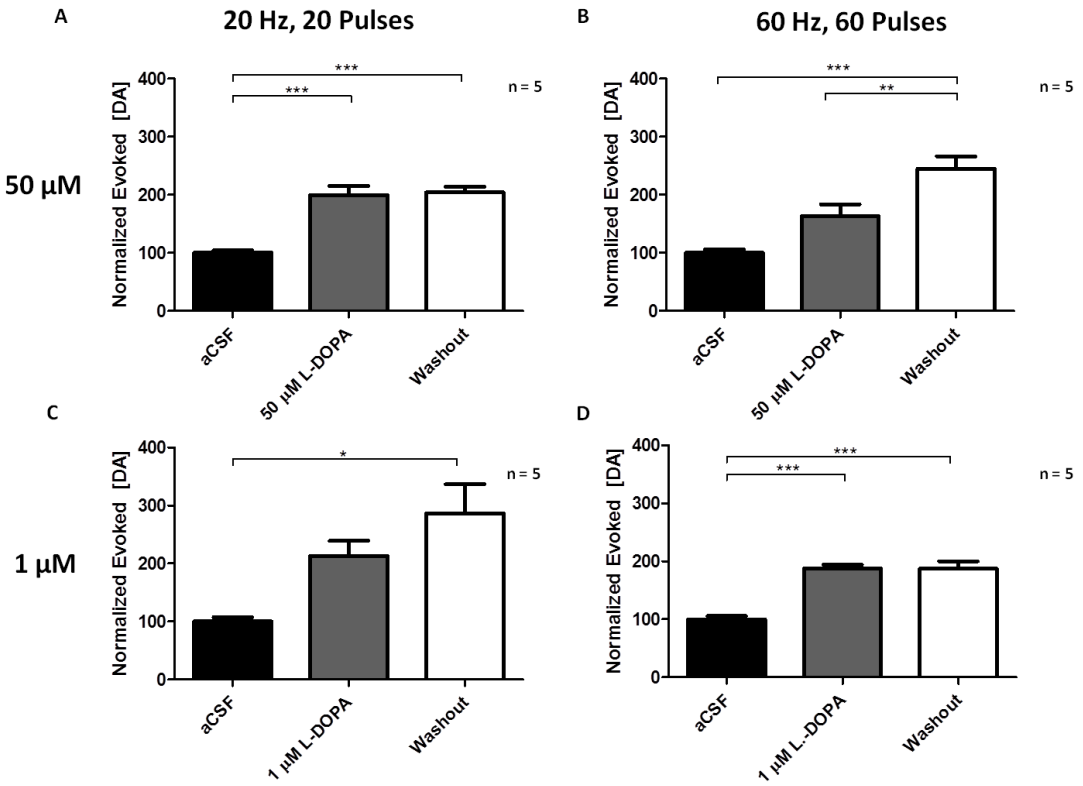

Figure 3.6 Assessment of Multiple Pulses at 20 and 60 Hz Frequencies of Evoked DA at Nafion-Coated Carbon-Fiber Microelectrodes. Data are expressed at +/- SEM ($P < 0.05$) evaluated with a one-way ANOVA and Tukey post-hoc comparison. (A) Electrically-evoked DA following a 20 Hz pulse train was significantly increased ($n = 5$) following 50 µM L-DOPA and in the washout step. (B) Electrically-evoked DA following a 60 Hz pulse train was significantly increased ($n = 5$) in the washout step. (C) Electrically-evoked DA following a 20 Hz pulse train was significantly increased ($n = 5$) in the washout step after 1 µM L-DOPA treatment. (D) Electrically-evoked DA following a 60 Hz pulse train was significantly increased ($n = 5$) following 1 µM L-DOPA and in the washout step.

Decreasing the concentration of L-DOPA to 1 µM did not significantly alter evoked DA release when using a 20 Hz pulse train, but did increase release when using the 60 Hz stimulation paradigm (Figure 3.6 C, D, $P < 0.05$, $n=5$). In both cases, DA release in the washout was significantly greater than the pre-drug value ($P< 0.05$, $n =5$). These data agree

with previously published work that shows that tonic excitation of DA neurons may not alter DA overflow.[12] Release and reuptake are tightly regulated. A stimulation frequency that is less than 20 Hz may not be sufficient to reveal the effects of 1 μM L-DOPA on DA release dynamics. Because the stimulation time was held constant, increases in DA overflow cannot be attributed to stimulation duration.[12] Rather, the response is a function of the number of pulses applied, as well as the frequency of the applied pulse train.

3.3.5 The Effect of L-DOPA on Dopamine Release and Reuptake Kinetics

The next set of experiments is aimed at quantitative assessment of the effects of L-DOPA on the kinetics of DA release and reuptake. DA release was electrically-evoked in striatal brain slice tissue using a 60 Hz stimulation paradigm before and after treatment with 1 μM L-DOPA. Data were collected using Nafion-coated carbon-fiber microelectrodes. These data were compared to a well-established mathematical model that uses the electrochemical form of the Michaelis-Menten (equation 3.1) in which the DAT is likened to the enzyme, and the DA in the extracellular space is the enzyme substrate.[12, 20] This is shown in Figure 3.1.

$$\frac{d[DA]}{dt} = [DA]_p f - \frac{V_{max}}{\left(\frac{K_m}{[DA]}+1\right)} \qquad (3.1)$$

Dopamine release corresponds to the rising phase of evoked DA signal and mean values of dopamine concentration released per stimulus pulse ($[DA]_p$) are determined from the maximum evoked DA. The falling phase corresponds to DA uptake, and decreases in V_{max} (maximal uptake rate of DA) will alter the slope of the falling phase.[12, 20] K_m describes the Michaelis constant for the affinity of dopamine for the dopamine transporter. For these

analyses K_m was held constant at 0.16 μM based on previous studies that utilized DA synaptosomes in the striatum.[18,19] Furthermore, L-DOPA does not compete with DA for the DAT.[29] The mean $[DA]_p$ was not altered by L-DOPA treatment , as shown in Figure 3.7 A.[30] This may be a dose-dependent response, and a different result may be evident when using a higher dose of L-DOPA. Indeed, 1 μM L-DOPA did not significantly increase the amplitude of DA release in the single pulse experiments in striatal brain slices (Figure 3.4 B-E and Figure 3.5). Thus, it is not surprising that the per pulse concentration of DA ($[DA]_p$) was not significantly different when calculated using the Michaelis-Menten model. In investigating V_{max}, however, a different result was found. Baseline electrical stimulations prior to L-DOPA treatment established a V_{max} value of 3.5 +/- 0.1 $\mu M \cdot s^{-1}$, a value that is comparable to other reports for the DAT V_{max} in the striatum.[30] However, treatment with 1 μM L-DOPA significantly decreased V_{max} (Figure 3.7 C, $P < 0.05$, $n = 5$). This value continued to decrease in the washout phase of the experiment ($P < 0.05$, $n = 5$). The fit of the kinetic model and the kinetic data for the analyses produced an average coefficient of determination of 0.87. These data are in agreement with a previous study using 60 μM L-DOPA in brain slice tissue that determined that L-DOPA decreases the clearance rate of DA following L-DOPA treatment.[15] This effect that may be due to DA's ability to inhibit its own uptake.[31] However, other voltammetric studies using high stimulus pulse trains and non-therapeutic doses of L-DOPA (greater than 60 μM in brain slice tissue and up to 250 $mg \cdot kg^{-1}$ in intact animals) have not shown L-DOPA to decrease V_{max}.[11-12] Changes in DA release and reuptake parameters may therefore be dose-dependent. Multiple doses should be assessed to

determine if there are changes in release and reuptake kinetics following pharmacological manipulation of brain tissue.

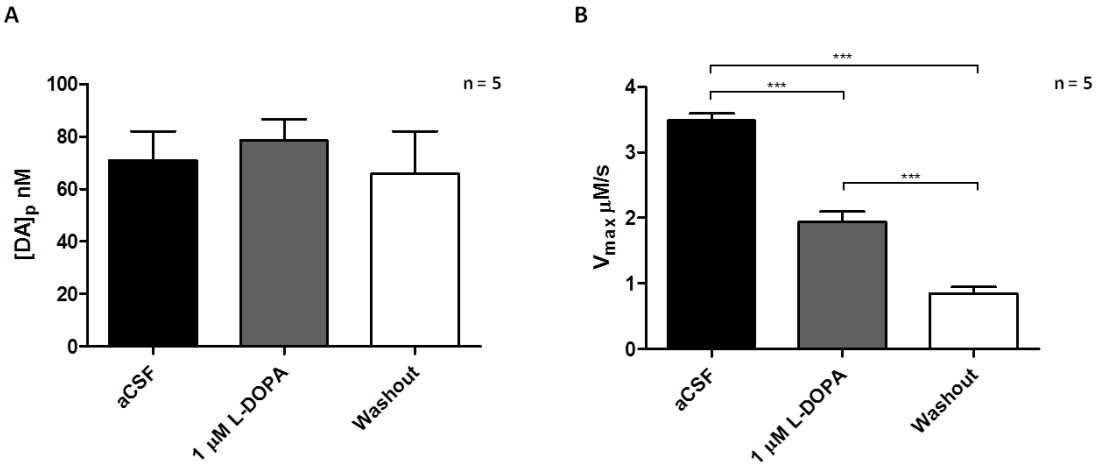

Figure 3.7 Kinetic Analysis of DA Release and Reuptake Parameters Following 1 µM L-DOPA Treatment. Data are presented at +/- SEM analyzed with one-way ANOVA and Tukey post-hoc comparison. (A) $[DA]_p$ (nM) of 60 Hz pulse train before and after 1 µM L-DOPA. There was no change in $[DA]_p$ after L-DOPA treatment. (B) V_{max} was significantly decreased following treatment with 1 µM L-DOPA and farther in the washout step ($P < 0.05$, n =5)

3.4 Conclusion

In conclusion, we have used FSCV at Nafion-coated carbon-fiber microelectrodes to examine electrically-evoked DA release in striatal brain slices following pharmacological manipulation with L-DOPA at various frequencies, applied pulses and L-DOPA concentrations. We have shown that L-DOPA hinders the detection of DA and fouls the

electrode surface. Increasing the applied pulses in the stimulation paradigm significantly increases the evoked DA in striatal slices with a lower concentration of L-DOPA (1 μM). At a more clinically relevant dose of L-DOPA (1 μM), DA reuptake is decreased, contrary to what has previously been reported. These data have provided an improved tool to monitor sub-second DA dynamics in living brain tissue and have indicated that with multiple pulses and at frequencies above 20 Hz (phasic firing), there is increased DA release at a lower, more clinically relevant dose than has previously been reported. Future work should focus on the phasic firing mode using a lower dose in 6-OHDA lesioned rats in order to establish sub-second DA dynamics in a decreased DA paradigm. Data such as these will inform us of changes in DA dynamics throughout the progression of PD and could potentially help us examine other potential pharmacotherapies.

REFERENCES CHAPTER 3

1. Dauer, W.; Przedborski, S., Parkinson's disease: mechanisms and models. *Neuron* **2003,** *39* (6), 889-909.

2. Hirsch, E.; Graybiel, A. M.; Agid, Y. A., Melanized dopaminergic neurons are differentially susceptible to degeneration in Parkinson's disease. *Nature* **1988,** *334* (6180), 345-8.

3. Jankovic, J., Parkinson's disease: clinical features and diagnosis. *J Neurol Neurosurg Psychiatry* **2008,** *79* (4), 368-76.

4. Shahed, J.; Jankovic, J., Motor symptoms in Parkinson's disease. *Handb Clin Neurol* **2007,** *83*, 329-42.

5. Jellinger, K. A., Pathology of Parkinson's disease. Changes other than the nigrostriatal pathway. *Mol Chem Neuropathol* **1991,** *14* (3), 153-97.

6. Dexter, D. T.; Jenner, P., Parkinson disease: from pathology to molecular disease mechanisms. *Free Radic Biol Med* **2013**.

7. Jenner, P., Molecular mechanisms of L-DOPA-induced dyskinesia. *Nat Rev Neurosci* **2008,** *9* (9), 665-77.

8. Lindgren, H. S.; Andersson, D. R.; Lagerkvist, S.; Nissbrandt, H.; Cenci, M. A., L-DOPA-induced dopamine efflux in the striatum and the substantia nigra in a rat model of Parkinson's disease: temporal and quantitative relationship to the expression of dyskinesia. *J Neurochem* **2010,** *112* (6), 1465-76.

9. Abercrombie, E. D.; Bonatz, A. E.; Zigmond, M. J., Effects of L-dopa on extracellular dopamine in striatum of normal and 6-hydroxydopamine-treated rats. *Brain Res* **1990,** *525* (1), 36-44.

10. Rodriguez, M.; Morales, I.; Gonzalez-Mora, J. L.; Gomez, I.; Sabate, M.; Dopico, J. G.; Rodriguez-Oroz, M. C.; Obeso, J. A., Different levodopa actions on the extracellular dopamine pools in the rat striatum. *Synapse* **2007,** *61* (2), 61-71.

11. May, L. J.; Kuhr, W. G.; Wightman, R. M., Differentiation of dopamine overflow and uptake processes in the extracellular fluid of the rat caudate nucleus with fast-scan in vivo voltammetry. *J Neurochem* **1988,** *51* (4), 1060-9.

12. Wightman, R. M.; Amatore, C.; Engstrom, R. C.; Hale, P. D.; Kristensen, E. W.; Kuhr, W. G.; May, L. J., Real-time characterization of dopamine overflow and uptake in the rat striatum. *Neuroscience* **1988,** *25* (2), 513-23.

13. Sombers, L. A.; Hanchar, H. J.; Colliver, T. L.; Wittenberg, N.; Cans, A.; Arbault, S.; Amatore, C.; Ewing, A. G., The effects of vesicular volume on secretion through the fusion pore in exocytotic release from PC12 cells. *J Neurosci* **2004,** *24* (2), 303-9.

14. Kennedy, R. T.; Jones, S. R.; Wightman, R. M., Simultaneous measurement of oxygen and dopamine: coupling of oxygen consumption and neurotransmission. *Neuroscience* **1992,** *47* (3), 603-12.

15. Jones, S. R.; Mickelson, G. E.; Collins, L. B.; Kawagoe, K. T.; Wightman, R. M., Interference by pH and Ca2+ ions during measurements of catecholamine release in slices of rat amygdala with fast-scan cyclic voltammetry. *J Neurosci Methods* **1994,** *52* (1), 1-10.

16. Cho, S.; Wood, A.; Bowlby, M. R., Brain slices as models for neurodegenerative disease and screening platforms to identify novel therapeutics. *Curr Neuropharmacol* **2007,** *5* (1), 19-33.

17. Robinson, D. L.; Hermans, A.; Seipel, A. T.; Wightman, R. M., Monitoring rapid chemical communication in the brain. *Chem Rev* **2008,** *108* (7), 2554-84.

18. Iverson, L. L., *Uptake Processes for Biogenic Amines* Plenum Pres: New York, 1975.

19. Iverson, L., Letter: High affinity uptake of neurotransmitter amino acids. *Nature* **1975,** *253* (5491), 481-2.

20. Yorgason, J. T.; Espana, R. A.; Jones, S. R., Demon voltammetry and analysis software: analysis of cocaine-induced alterations in dopamine signaling using multiple kinetic measures. *J Neurosci Methods* **2011,** *202* (2), 158-64.

21. Grace, A. A.; Bunney, B. S., The control of firing pattern in nigral dopamine neurons: single spike firing. *J Neurosci* **1984,** *4* (11), 2866-76.

22. Sombers, L. A.; Beyene, M.; Carelli, R. M.; Wightman, R. M., Synaptic overflow of dopamine in the nucleus accumbens arises from neuronal activity in the ventral tegmental area. *J Neurosci* **2009,** *29* (6), 1735-42.

23. Stuber, G. D.; Klanker, M.; de Ridder, B.; Bowers, M. S.; Joosten, R. N.; Feenstra, M. G.; Bonci, A., Reward-predictive cues enhance excitatory synaptic strength onto midbrain dopamine neurons. *Science* **2008,** *321* (5896), 1690-2.

24. Wanat, M. J.; Willuhn, I.; Clark, J. J.; Phillips, P. E., Phasic dopamine release in appetitive behaviors and drug addiction. *Curr Drug Abuse Rev* **2009,** *2* (2), 195-213.

25. McCutcheon, J. E.; Beeler, J. A.; Roitman, M. F., Sucrose-predictive cues evoke greater phasic dopamine release than saccharin-predictive cues. *Synapse* **2012,** *66* (4), 346-51.

26. Hashemi, P.; Dankoski, E. C.; Petrovic, J.; Keithley, R. B.; Wightman, R. M., Voltammetric detection of 5-hydroxytryptamine release in the rat brain. *Anal Chem* **2009,** *81* (22), 9462-71.

27. Lundblad, M.; af Bjerken, S.; Cenci, M. A.; Pomerleau, F.; Gerhardt, G. A.; Stromberg, I., Chronic intermittent L-DOPA treatment induces changes in dopamine release. *J Neurochem* **2009,** *108* (4), 998-1008.

28. Xu, K.; Dluzen, D. E., L-DOPA modulation of corpus striatal dopamine and dihydroxyphenylacetic acid output from intact and 6-OHDA lesioned rats. *J Neural Transm* **1996,** *103* (11), 1295-305.

29. Fernagut, P. O.; Li, Q.; Dovero, S.; Chan, P.; Wu, T.; Ravenscroft, P.; Hill, M.; Chen, Z.; Bezard, E., Dopamine transporter binding is unaffected by L-DOPA administration in normal and MPTP-treated monkeys. *PLoS One* **2010,** *5* (11), e14053.

30. Bunin, M. A.; Wightman, R. M., Measuring uptake rates in intact tissue. *Methods Enzymol* **1998,** *296*, 689-707.

31. Richelson, E.; Pfenning, M., Blockade by antidepressants and related compounds of biogenic amine uptake into rat brain synaptosomes: most antidepressants selectively block norepinephrine uptake. *Eur J Pharmacol* **1984,** *104* (3-4), 277-86.

APPENDICES

Appendix A

Glossary of Abbreviations

3-MT	3-methoxytyramine. A metabolite of dopamine.
6-OHDA	6-hydroxydopamine. A neurotoxic compound used to selectively destroy dopaminergic neurons to induce Parkinsonian-like symptoms in animal models.
AADC	L-aromatic amino acid decarboxylase, also known as DOPA decarboxylase. An enzyme that catalyzes the decarboxylation of various reactions including L-DOPA to dopamine.
ADC	Analog-to-digital converter. A device that converts analog signals to digital signals.
aCSF	Artificial cerebrospinal fluid. A mimetic biological matrix that envelops the brain and spinal cord composed of various salts used as a buffer in electrochemical studies.
AD	Alzheimer's Disease. A neurodegenerative disease that destroys memory and cognitive functions.
ATP	Adenosine triphosphate. A nucleotide triphosphate used to transport chemical energy within cells for metabolism.
CFME	Carbon-fiber microelectrode. An electrode composed of a single carbon-fiber cut to a specified length typically 6-7 μm in diameter and 100-400 μm in length, typically sealed in a glass capillary tube used to measure neurochemicals *in-vivo* and *in-vitro*.

COMT	Catechol-o-methyl transferase. One of several enzymes that catabolizes dopamine into its metabolites.
[DA]	Instantaneous concentration of extracellular dopamine.
$[DA]_p$	Dopamine concentration release per stimulus pulse. A measure of dopamine release assessed with Michaelis-Menten kinetics.
DA	Dopamine. A monoamine neurotransmitter with various important functions including involvement in reward and addiction and movement within the brain.
DAC	Digital-to-analog converter. A device that converts digital signals to analog signals.
DAT	Dopamine transporter. An integral membrane protein of dopamine neurons responsible for the active reuptake of dopamine in the extracellular space.
DOPAC	3,4-Dihydroxyphenylacetic acid. A metabolite of dopamine.
DNA	Deoxyribonucleic acid. A molecule that encodes all of the genetic information necessary for development and function in all living organisms.
ECE	Electrochemical-chemical-electrochemical reaction.
FSCV	Fast-scan cyclic voltammetry. An electrochemical technique in which the potential is varied linearly at a very fast sweep rate.
H_2O_2	Hydrogen peroxide.

HEPES	4-(2-hydroxyethyl)-1-piperazineethanesulfonic acid. A zwitterionic chemical buffering agent commonly used to help maintain cell cultures and living tissue viable by maintaining physiological pH.
HPLC	High-performance liquid chromatography. A chromatographic technique used to identify and quantify an analyte of interest.
HVA	3-Methoxy-4-hydroxyphenylactic acid or homovanillic acid. A metabolite of dopamine.
IUACUC	Institutional Animal Care and Use Committee.
K^+	Potassium ion.
K_m	The Michaelis constant. A measure of the affinity of a substrate for the enzyme. It is defined as one-half of the maximum reuptake rate achieved by the system.
LAT	Large amino acid transporter. A protein responsible for the transport of L-DOPA across the blood-brain-barrier.
L-DOPA	L-3,4-Dihydroxyphenylalanine. The precursor molecule to dopamine and gold standard therapy of Parkinson's Disease.
MAO	Monoamine oxidase. An enzyme responsible for the catabolism of dopamine.
MPP^+	1-methyl-4-phenylpyridinium. A chemical toxin that causes Parkinsonism by interfering with oxidative phosphorylation in mitochondria and depletion of ATP leading to cell death.
MPTP	1-Methyl-4-phenyl-1,2,3,6-tetrahydropyridine. A neurotoxin precursor to MPP^+ used to cause symptoms of Parkinson's disease in animal models.

Na^+	Sodium ion.
NOS	Nitric oxide synthase. A family of enzymes that catalyze the production of nitric oxide from L-arginine.
NO	Nitric oxide. A free radical molecule produced from NOS that an important signaling both peripherally and in the brain.
PD	Parkinson's Disease. A neurodegenerative disease resulting from the selective loss of dopaminergic neurons in the substantia nigra that project to the dorsal striatum. It is characterized by motor abnormalities.
RNS	Reactive nitrogen species. A family of molecules derived from nitric oxide and superoxide anion that are highly reactive and can cause nitrosative and oxidative stress.
ROS	Reactive oxygen species. Oxygen containing molecules derived from the metabolism of oxygen that are involved in cellular function and chemical modulation and can cause oxidative stress leading to cell death.
SEM	Scanning Electron Microscope. An electron microscope that obtains sample images by scanning a sample with a focused beam of electrons, generally in a vacuum.
SN	Substantia nigra. A brain structure that is part of the mesencephalon and the location of cell degeneration in Parkinson's disease.
TH	Tyrosine hydroxylase. An enzyme that catalyzes the conversion of tyrosine to L-DOPA.
VMAT	Vesicular monoamine transporter. A protein present in presynaptic neurons that transports monoamines into synaptic vesicles.

V_{max}	The maximum uptake rate achieved by an enzymatic reaction at maximum saturating concentrations.